International Journal of Plasticity 27 (2011) 940–961

Contents lists available at ScienceDirect

International Journal of Plasticity

journal homepage: www.elsevier.com/locate/ijplas

A finite strain kinematic hardening constitutive model based on Hencky strain: General framework, solution algorithm and application to shape memory alloys

J. Arghavani [a,1], F. Auricchio [b,c,d], R. Naghdabadi [a,e,*]

[a] Department of Mechanical Engineering, Sharif University of Technology, 11155-9567 Tehran, Iran
[b] Dipartimento di Meccanica Strutturale, Università degli Studi di Pavia, Pavia, Italy
[c] Center for Advanced Numerical Simulation (CeSNA), IUSS, Pavia, Italy
[d] European Centre for Training and Research in Earthquake Engineering (EUCENTRE), Pavia, Italy
[e] Institute for Nano-Science and Technology, Sharif University of Technology, 11155-9567 Tehran, Iran

ARTICLE INFO

Article history:
Received 30 August 2010
Received in final revised form 6 September 2010
Available online 4 November 2010

Keywords:
Logarithmic strain
Shape memory alloys
Kinematic hardening
Logarithmic mapping
Multiplicative decomposition

ABSTRACT

The logarithmic or Hencky strain measure is a favored measure of strain due to its remarkable properties in large deformation problems. Compared with other strain measures, e.g., the commonly used Green–Lagrange measure, logarithmic strain is a more physical measure of strain. In this paper, we present a Hencky-based phenomenological finite strain kinematic hardening, non-associated constitutive model, developed within the framework of irreversible thermodynamics with internal variables. The derivation is based on the multiplicative decomposition of the deformation gradient into elastic and inelastic parts, and on the use of the isotropic property of the Helmholtz strain energy function. We also use the fact that the corotational rate of the Eulerian Hencky strain associated with the so-called logarithmic spin is equal to the strain rate tensor (symmetric part of the velocity gradient tensor). Satisfying the second law of thermodynamics in the Clausius–Duhem inequality form, we derive a thermodynamically-consistent constitutive model in a Lagrangian form. In comparison with the available finite strain models in which the unsymmetric Mandel stress appears in the equations, the proposed constitutive model includes only symmetric variables. Introducing a logarithmic mapping, we also present an appropriate form of the proposed constitutive equations in the time-discrete frame. We then apply the developed constitutive model to shape memory alloys and propose a well-defined, non-singular definition for model variables. In addition, we present a nucleation-completion condition in constructing the solution algorithm. We finally solve several boundary value problems to demonstrate the proposed model features as well as the numerical counterpart capabilities.

1. Introduction

In recent years much attention has been devoted to the development of constitutive laws for large deformations of solids. The logarithmic strain, sometimes referred to as true or natural strain, introduced by Hencky (1928) and also called Hencky

* Corresponding author at: Department of Mechanical Engineering, Sharif University of Technology, 11155-9567 Tehran, Iran. Tel.: +98 21 6616 5546; fax: +98 21 6600 0021.
E-mail address: naghdabd@sharif.edu (R. Naghdabadi).
[1] Currently visiting Ph. D. student, Dipartimento di Meccanica Strutturale, Universit'a degli Studi di Pavia, Italy.

0749-6419/$ - see front matter © 2010 Elsevier Ltd. All rights reserved.
doi:10.1016/j.ijplas.2010.10.006

strain, is a favored measure of strain due to its remarkable properties at large deformations in solid mechanics, materials science and metallurgy. A remarkable property is that among all finite strain measures, only the spherical and the deviatoric parts of the Hencky strain can, in an additive manner, separate the volumetric deformation and the isochoric deformation from the total deformation, whereas the just-mentioned two deformation modes are inseparably coupled with each other in either of the spherical part and the deviatoric part of any other strain measure (Xiao et al., 2004).

Moreover, the logarithmic strain possesses certain intrinsic far-reaching properties that establish its favored position in all possible strain measures. One reason of such properties was clarified by disclosing an important relation, i.e., the Eulerian logarithmic strain is the unique strain measure that its corotational rate (associated with the so-called logarithmic spin) is the strain rate tensor. In other words, the strain rate tensor, $\boldsymbol{d}$, is the corotational rate of the Hencky strain tensor associated with the logarithmic spin tensor. Such a result has been introduced by Reinhardt and Dubey (1995) as D-rate and by Xiao et al. (1997) as log-rate. The work-conjugate pair of Eulerian Hencky strain and Cauchy stress, being natural or true strain and stress measures, respectively, are of most interest in constitutive modeling beyond the small strain regime (Xiao et al., 2006).

For its considerable advantages, logarithmic strain has been used in constitutive modeling of solids by many authors (see, e.g., Xiao et al., 2000, 2001; Bruhns et al., 1999; Yeganeh and Naghdabadi, 2006; Naghdabadi et al., 2005; Peric et al., 1992; Reinhardt and Dubey, 1996; Criscione et al., 2000; Miehe et al., 2002; Lin and Schomburg, 2003; Xiao and Chen, 2002; Müller and Bruhns, 2006).

There has also been a lot of effort in the literature using Green–Lagrange strain and the second Piola–Kirchhoff stress which are finite strain and stress as well as work-conjugate measures in nonlinear solid mechanics. However, the physical meaning of Green–Lagrange strain is not precise and direct unless the magnitude is small. Sometimes Green–Lagrange strain is called an energy-measure strain (Pai and Palazotto, 1998) to emphasis that it is not a physical or true measure.

Recently, Darijani and Naghdabadi (2010) have reconsidered the strain measure definition to satisfy the consistency requirements: (1) strain should go to $+\infty$ when stretch goes to $+\infty$. This means that under a very large stretching condition, strain should take a very large positive value, (2) strain should go to $-\infty$ when stretch goes to zero. This means that under a high compression condition, strain should take a very large negative value. As discussed by Darijani and Naghdabadi, the well known Seth-Hill strain measures do not satisfy the both requirements simultaneously.[2] We emphasis that the Hencky strain, belonging to both Seth-Hill and Darijani–Naghdabadi measures, is the only member of Seth-Hill class that satisfies both requirements.

There are still more motivations to develop a Hencky-strain based constitutive model. For example, for a Hookean-type constitutive relation, only the Hencky-based one is useful at moderately large elastic stretches (Anand, 1979, 1986). Another motivation is related to the physical kinematical constraints, for instance, in shape memory alloys (SMAs), to capture the transformation-induced strain saturation, it is necessary to define a kinematical constraint on the inelastic true strain norm. This constraint has so far been enforced through the Green–Lagrange strain norm. However, the use of Green–Lagrange strain is reasonable for small strain, large rotation deformations. Moreover, the incompressibility constraint takes a very simple form when Hencky strain is used (Xiao et al., 2004).

In this study, based on the Hencky strain, we develop a finite strain constitutive model. To this end, the paper is organized as follows. Section 2 presents some preliminaries. In Section 3, based on a multiplicative decomposition of the deformation gradient into elastic and inelastic parts, we present a finite-strain non-associative constitutive model. In Section 4, we introduce a logarithmic mapping to propose the time-discrete constitutive model. In Section 5, we apply the developed constitutive model to shape memory alloys and solve several boundary value problems in Section 6. We finally draw conclusions in Section 7.

2. Preliminaries

According to the polar decomposition theorem, the deformation gradient $\boldsymbol{F}$ with $J = \det(\boldsymbol{F}) > 0$ is uniquely decomposed as

$$\boldsymbol{F} = \boldsymbol{R}\boldsymbol{U} = \boldsymbol{V}\boldsymbol{R}, \tag{1}$$

where $\boldsymbol{R}$ is a proper orthogonal tensor and $\boldsymbol{U}$ and $\boldsymbol{V}$ are symmetric positive definite right and left stretch tensors, respectively.

A multiplicative decomposition of $\boldsymbol{F}$ into dilatational and distortional parts is defined as

$$\boldsymbol{F} = \left(J^{1/3}\mathbf{1}\right)\overline{\boldsymbol{F}} = J^{1/3}\overline{\boldsymbol{F}}, \tag{2}$$

where $\mathbf{1}$ is the second-order identity tensor, and $\det(\overline{\boldsymbol{F}}) = 1$. The terms $J^{1/3}\mathbf{1}$ and $\overline{\boldsymbol{F}}$ are associated, respectively, with volume-changing and volume-preserving deformations of the material (Holzapfel, 2000).

Then, the right and left Cauchy–Green deformation tensors are, respectively, defined as

$$\begin{aligned} \boldsymbol{C} &= \boldsymbol{F}^T\boldsymbol{F} = \boldsymbol{U}^2 = J^{2/3}\overline{\boldsymbol{F}}^T\overline{\boldsymbol{F}} = J^{2/3}\overline{\boldsymbol{C}} = J^{2/3}\overline{\boldsymbol{U}}^2, \\ \boldsymbol{b} &= \boldsymbol{F}\boldsymbol{F}^T = \boldsymbol{V}^2 = J^{2/3}\overline{\boldsymbol{F}}\overline{\boldsymbol{F}}^T = J^{2/3}\bar{\boldsymbol{b}} = J^{2/3}\overline{\boldsymbol{V}}^2, \end{aligned} \tag{3}$$

where $\det(\overline{\boldsymbol{C}}) = \det(\overline{\boldsymbol{U}}) = 1$ and $\det(\bar{\boldsymbol{b}}) = \det(\overline{\boldsymbol{V}}) = 1$.

[2] For example, Green–Lagrange strain measure, $\boldsymbol{E} = \frac{1}{2}(\boldsymbol{U}^2 - \mathbf{1}) \to -\frac{1}{2}\mathbf{1}$ when $\boldsymbol{U} \to \mathbf{0}$.

The material and spatial Hencky (or logarithmic) strain tensors $\boldsymbol{H}$ and $\boldsymbol{h}$ read, respectively, as (Lubarda, 2002)[3]:

$$\begin{aligned}\boldsymbol{H} &= \log \boldsymbol{U} = \frac{1}{2}\log \boldsymbol{C} = \overline{\boldsymbol{H}} + \frac{1}{3}\theta \mathbf{1},\\ \boldsymbol{h} &= \log \boldsymbol{V} = \frac{1}{2}\log \boldsymbol{b} = \bar{\boldsymbol{h}} + \frac{1}{3}\theta \mathbf{1},\end{aligned} \tag{4}$$

where

$$\theta = \log(J), \quad \overline{\boldsymbol{H}} = \log \overline{\boldsymbol{U}} = \frac{1}{2}\log \overline{\boldsymbol{C}}, \quad \bar{\boldsymbol{h}} = \log \overline{\boldsymbol{V}} = \frac{1}{2}\log \bar{\boldsymbol{b}}, \tag{5}$$

Moreover, the velocity gradient tensor $\boldsymbol{l}$ is given as

$$\boldsymbol{l} = \dot{\boldsymbol{F}}\boldsymbol{F}^{-1} = \bar{\boldsymbol{l}} + \frac{1}{3}\dot{\theta}\mathbf{1}, \tag{6}$$

where

$$\bar{\boldsymbol{l}} = \dot{\overline{\boldsymbol{F}}}\overline{\boldsymbol{F}}^{-1}, \tag{7}$$

The symmetric and skew symmetric parts of $\boldsymbol{l}$ supply, respectively, the strain rate tensor $\boldsymbol{d}$ and the vorticity tensor $\boldsymbol{w}$, i.e.

$$\begin{aligned}\boldsymbol{d} &= \mathrm{sym}(\boldsymbol{l}) = \bar{\boldsymbol{d}} + \frac{1}{3}\dot{\theta}\mathbf{1},\\ \boldsymbol{w} &= \mathrm{skew}(\boldsymbol{l}) = \bar{\boldsymbol{w}},\end{aligned} \tag{8}$$

where $\bar{\boldsymbol{d}} = \mathrm{sym}(\bar{\boldsymbol{l}})$ and $\bar{\boldsymbol{w}} = \mathrm{skew}(\bar{\boldsymbol{l}})$, while $\mathrm{sym}(\boldsymbol{A}) = (1/2)(\boldsymbol{A} + \boldsymbol{A}^T)$ and $\mathrm{skew}(\boldsymbol{A}) = (1/2)(\boldsymbol{A} - \boldsymbol{A}^T)$ compute the symmetric and skew symmetric parts of an arbitrary tensor $\boldsymbol{A}$, respectively.

Taking the time derivative of relation $\boldsymbol{C} = \boldsymbol{F}^T\boldsymbol{F}$ and using $(6)_1$ and $(8)_1$, it can be shown that:

$$\dot{\boldsymbol{C}} = 2\boldsymbol{F}^T\boldsymbol{d}\boldsymbol{F}, \tag{9}$$

Corotational rate of an Eulerian tensor $\mathcal{A}$ associated with the rotating frame having spin $\boldsymbol{\Omega}$ is defined as

$$\overset{\circ}{\mathcal{A}} = \dot{\mathcal{A}} - \boldsymbol{\Omega}\mathcal{A} + \mathcal{A}\boldsymbol{\Omega}, \tag{10}$$

where $\dot{\mathcal{A}}$ is the material time derivative of $\mathcal{A}$ associated with the fixed frame and $\overset{\circ}{\mathcal{A}}$ is the corotational rate of $\mathcal{A}$ (Xiao et al., 1997; Ghavam and Naghdabadi, 2007).

We now double contract both sides of (10) with an arbitrary second-order symmetric tensor $\mathcal{B}$; assuming $\mathcal{A}$ symmetric and after some mathematical manipulation, we obtain:

$$\overset{\circ}{\mathcal{A}} : \mathcal{B} = \dot{\mathcal{A}} : \mathcal{B} + 2\boldsymbol{\Omega} : (\mathcal{A}\mathcal{B}), \tag{11}$$

where: indicates double contraction, defined as $\boldsymbol{A} : \boldsymbol{B} = A_{ij}B_{ij}$ for second-order tensors.

If $\mathcal{A}$ and $\mathcal{B}$ are coaxial (besides being symmetric), $\mathcal{A}\mathcal{B}$ is also symmetric and its double contraction with the skew-symmetric tensor $\boldsymbol{\Omega}$ vanishes. Therefore, we conclude the following identity for any arbitrary spin tensor $\boldsymbol{\Omega}$:

$$\text{if } \mathcal{A} \text{ and } \mathcal{B} \text{ are symmetric and coaxial } \Rightarrow \ \dot{\mathcal{A}} : \mathcal{B} = \overset{\circ}{\mathcal{A}} : \mathcal{B}. \tag{12}$$

The corotational rate of the Eulerian (or spatial) Hencky strain $\boldsymbol{h}$ associated with the so-called logarithmic spin[4] $\boldsymbol{\Omega}^{log}$ is identical to the Eulerian stretching $\boldsymbol{d}$, and $\boldsymbol{h}$ is the only strain enjoying this property (Xiao et al., 1997). According to (10), this means:

$$\overset{\circ}{\boldsymbol{h}}^{log} = \dot{\boldsymbol{h}} - \boldsymbol{\Omega}^{log}\boldsymbol{h} + \boldsymbol{h}\boldsymbol{\Omega}^{log} = \boldsymbol{d}. \tag{13}$$

3. A kinematic hardening constitutive model based on Hencky strain

In this section, we use the multiplicative decomposition of the deformation gradient into elastic and inelastic parts and, defining Helmholtz strain energy function in terms of elastic and inelastic Hencky strains, we develop a thermodynamically-consistent finite strain kinematic hardening constitutive model.

[3] The material and spatial Hencky strains are computed through spectral decomposition, i.e.,

$$\boldsymbol{H} = \sum_{i=1}^{3}\log(\lambda_i)\boldsymbol{e}_i \otimes \boldsymbol{e}_i \quad \text{and} \quad \boldsymbol{h} = \sum_{i=1}^{3}\log(\lambda_i)\bar{\boldsymbol{e}}_i \otimes \bar{\boldsymbol{e}}_i,$$

where λ_i are the three principal stretches (possibly repeated), while $\boldsymbol{e}_i$ and $\bar{\boldsymbol{e}}_i$ are the corresponding principal directions of the right and left stretch tensors, respectively.

[4] In this study, only the existence of such spin is utilized and the explicit form of $\boldsymbol{\Omega}^{log}$ is not needed; however we refer to e.g., Reinhardt and Dubey (1995), Xiao et al. (1997), Ghavam and Naghdabadi (2007) for more details.

3.1. Constitutive model development

Following a well-established approach adopted in plasticity (Lubarda, 2002; Haupt, 2002) and already used for SMAs (see, e.g., Helm, 2001; Auricchio, 2001; Ziolkowski, 2007; Reese and Christ, 2008; Christ and Reese, 2009; Arghavani et al., 2010d,; Thamburaja, 2010 among others), we assume a multiplicative decomposition of the deformation gradient into an elastic part $\boldsymbol{F}^e$, defined with respect to an intermediate configuration, and an inelastic one $\boldsymbol{F}^{in}$, defined with respect to the reference configuration,[5] i.e.

$$\boldsymbol{F} = \boldsymbol{F}^e \boldsymbol{F}^{in}. \tag{14}$$

Moreover, we utilize the deformation gradient decomposition into volumetric and distortional parts, as follows:

$$\begin{aligned} \boldsymbol{F}^e &= J^{e\frac{1}{3}} \overline{\boldsymbol{F}}^e, \\ \boldsymbol{F}^{in} &= J^{in\frac{1}{3}} \overline{\boldsymbol{F}}^{in}, \end{aligned} \tag{15}$$

where $J^e = \det(\boldsymbol{F}^e)$, $J^{in} = \det(\boldsymbol{F}^{in})$ and $\det(\overline{\boldsymbol{F}}^e) = \det(\overline{\boldsymbol{F}}^{in}) = 1$.

Similarly, we may define the following tensors:

$$\begin{aligned} &\boldsymbol{C}^e = \boldsymbol{F}^{e^T}\boldsymbol{F}^e, \quad \overline{\boldsymbol{C}}^e = \overline{\boldsymbol{F}}^{e^T}\overline{\boldsymbol{F}}^e, \quad \boldsymbol{b}^e = \boldsymbol{F}^e\boldsymbol{F}^{e^T}, \quad \bar{\boldsymbol{b}}^e = \overline{\boldsymbol{F}}^e\overline{\boldsymbol{F}}^{e^T}, \\ &\boldsymbol{C}^{in} = \boldsymbol{F}^{in^T}\boldsymbol{F}^{in}, \quad \overline{\boldsymbol{C}}^{in} = \overline{\boldsymbol{F}}^{in^T}\overline{\boldsymbol{F}}^{in}, \quad \boldsymbol{b}^{in} = \boldsymbol{F}^{in}\boldsymbol{F}^{in^T}, \quad \bar{\boldsymbol{b}}^{in} = \overline{\boldsymbol{F}}^{in}\overline{\boldsymbol{F}}^{in^T}, \\ &\boldsymbol{U}^e = \boldsymbol{C}^{e^{1/2}}, \quad \overline{\boldsymbol{U}}^e = \overline{\boldsymbol{C}}^{e^{1/2}}, \quad \boldsymbol{V}^e = \boldsymbol{b}^{e^{1/2}}, \quad \overline{\boldsymbol{V}}^e = \bar{\boldsymbol{b}}^{e^{1/2}}, \\ &\boldsymbol{U}^{in} = \boldsymbol{C}^{in^{1/2}}, \quad \overline{\boldsymbol{U}}^{in} = \overline{\boldsymbol{C}}^{in^{1/2}}, \quad \boldsymbol{V}^{in} = \boldsymbol{b}^{in^{1/2}}, \quad \overline{\boldsymbol{V}}^{in} = \bar{\boldsymbol{b}}^{in^{1/2}}, \\ &\boldsymbol{H}^e = \log \boldsymbol{U}^e, \quad \overline{\boldsymbol{H}}^e = \log \overline{\boldsymbol{U}}^e, \quad \boldsymbol{H}^{in} = \log \boldsymbol{U}^{in}, \quad \overline{\boldsymbol{H}}^{in} = \log \overline{\boldsymbol{U}}^{in}, \end{aligned} \tag{16}$$

Combining (14) and (15), we obtain:

$$\boldsymbol{F} = (J^e J^{in})^{\frac{1}{3}} \overline{\boldsymbol{F}}^e \overline{\boldsymbol{F}}^{in} = J^{\frac{1}{3}} \overline{\boldsymbol{F}}, \tag{17}$$

where

$$J = J^e J^{in} \quad \text{and} \quad \overline{\boldsymbol{F}} = \overline{\boldsymbol{F}}^e \overline{\boldsymbol{F}}^{in}. \tag{18}$$

Substituting (18) into $(8)_1$, we obtain:

$$\bar{\boldsymbol{d}} = \dot{\overline{\boldsymbol{F}}}\overline{\boldsymbol{F}}^{-1} = \bar{\boldsymbol{d}}^e + \operatorname{sym}\left(\overline{\boldsymbol{F}}^e \bar{\boldsymbol{l}}^{in} \overline{\boldsymbol{F}}^{e^{-1}}\right) \quad \text{and} \quad \theta = \theta^e + \theta^{in}, \tag{19}$$

where, $\bar{\boldsymbol{d}}^e = \operatorname{sym}(\dot{\overline{\boldsymbol{F}}}^e \overline{\boldsymbol{F}}^{e^{-1}})$, $\bar{\boldsymbol{l}}^{in} = \dot{\overline{\boldsymbol{F}}}^{in} \overline{\boldsymbol{F}}^{in^{-1}}$, $\theta^e = log(J^e)$ and $\theta^{in} = \log(J^{in})$.

In order to satisfy the principle of material objectivity, the Helmholtz free energy has to depend on $\boldsymbol{F}^e$ only through the elastic right stretch tensor; it is moreover assumed to be a function of $\boldsymbol{F}^{in}$ through the inelastic right stretch tensor and of the temperature,[6] T. Finally, we express the Helmholtz free energy per unit undeformed volume, decomposed additively in the following form:

$$\Psi = \Psi\left(\theta^e, \theta^{in}, \overline{\boldsymbol{H}}^e, \overline{\boldsymbol{H}}^{in}, T\right) = \phi^e(\theta^e) + \psi^e(\overline{\boldsymbol{H}}^e) + \phi^{in}(\theta^{in}) + \psi^{in}(\overline{\boldsymbol{H}}^{in}, T) = W^e(\boldsymbol{H}^e) + W^{in}(\boldsymbol{H}^{in}, T), \tag{20}$$

where $W^e(\boldsymbol{H}^e)$ is a hyperelastic strain energy function decomposed into $\phi^e(\theta^e)$ and $\psi^e(\overline{\boldsymbol{H}}^e)$, representing the volumetric and distorsional elastic strain energies due to the elastic material deformations, respectively. Similarly, the term $W^{in}(\boldsymbol{H}^{in},T)$ represents the additional amount of stored energy due to inelastic hardening (e.g., phase transformation, plastic hardening and so on), decomposed into volumetric and isochoric parts $\phi^{in}(\theta^{in})$ and $\psi^{in}(\overline{\boldsymbol{H}}^{in})$, respectively. For simplicity we do not consider the isotropic hardening effect, knowing that it can be easily included in the proposed constitutive model.

In this study, we assume $\psi^e(\overline{\boldsymbol{H}}^e)$ and $\psi^{in}(\overline{\boldsymbol{H}}^{in}, T)$ to be isotropic functions of $\overline{\boldsymbol{H}}^e$ and $\overline{\boldsymbol{H}}^{in}$, respectively.[7] Therefore, ψ^e and ψ^{in} can be expressed as functions of their argument invariants. Since, the Lagrangian and Eulerian Hencky strains have the same invariants, we can express the Helmholtz free energy as a function of the Eulerian Hencky strains, i.e.

$$\Psi\left(\theta^e, \theta^{in}, \overline{\boldsymbol{H}}^e, \overline{\boldsymbol{H}}^{in}, T\right) = \Psi\left(\theta^e, \theta^{in}, \bar{\boldsymbol{h}}^e, \bar{\boldsymbol{h}}^{in}, T\right) = \phi^e(\theta^e) + \psi^e(\bar{\boldsymbol{h}}^e) + \phi^{in}(\theta^{in}) + \psi^{in}(\bar{\boldsymbol{h}}^{in}, T), \tag{21}$$

We now use Clausius–Duhem inequality form of the second law of thermodynamics:

$$J\boldsymbol{\sigma} : \boldsymbol{d} - (\dot{\Psi} + \eta\dot{T}) = \boldsymbol{\tau} : \boldsymbol{d} - (\dot{\Psi} + \eta\dot{T}) \geqslant 0, \tag{22}$$

[5] We use inelastic terminology which is more general. For example when talking about plasticity, we can use $\boldsymbol{F}^{in} = \boldsymbol{F}^p$ and when we are interested in SMA modeling, the inelasticity is due to phase transformation and we can use $\boldsymbol{F}^{in} = \boldsymbol{F}^t$.

[6] We remark that we do not consider a fully thermo-mechanical coupled model. In this way, the Helmholtz free energy should be more properly referred to as a temperature-parameterized function.

[7] We refer to Henann and Anand (2009) and Gurtin and Anand (2005) for more details on objectivity as well as isotropy requirements.

where η is the entropy and $\boldsymbol{\tau} = J\boldsymbol{\sigma}$ is the Kirchhoff stress tensor.

Moreover, we make use of $(8)_1$ and the additive decomposition of the Kirchhoff stress tensor $\boldsymbol{\tau}$ into a hydrostatic part $p\mathbf{1}$ and a deviatoric part: $\boldsymbol{s} = \boldsymbol{\tau} - p\mathbf{1}$, where $p = \mathrm{tr}\,(\boldsymbol{\tau})/3$, and rewrite (22) as

$$p\dot{\theta} + \boldsymbol{s} : \bar{\boldsymbol{d}} - (\dot{\Psi} + \eta\dot{T}) \geqslant 0. \tag{23}$$

We now substitute (19) and (21) into (23) to obtain:

$$p\left(\dot{\theta}^e + \dot{\theta}^{in}\right) + \boldsymbol{s} : \left[\bar{\boldsymbol{d}}^e + \mathrm{sym}\left(\overline{\boldsymbol{F}}^e\bar{\boldsymbol{l}}^{in}\overline{\boldsymbol{F}}^{e^{-1}}\right)\right] - \left(\frac{\partial\phi^e}{\partial\theta^e}\dot{\theta}^e + \frac{\partial\psi^e}{\partial\bar{\boldsymbol{h}}^e} : \dot{\bar{\boldsymbol{h}}}^e + \frac{\partial\phi^{in}}{\partial\theta^{in}}\dot{\theta}^{in} + \frac{\partial\psi^{in}}{\partial\bar{\boldsymbol{h}}^{in}} : \dot{\bar{\boldsymbol{h}}}^{in} + \frac{\partial\psi^{in}}{\partial T}\dot{T}\right) - \eta\dot{T} \geqslant 0. \tag{24}$$

As a consequence of isotropy, the symmetric tensors $\bar{\boldsymbol{h}}^e$ and $\partial\psi^e/\partial\bar{\boldsymbol{h}}^e$ as well as the symmetric tensors $\bar{\boldsymbol{h}}^{in}$ and $\partial\psi^{in}/\partial\bar{\boldsymbol{h}}^{in}$ are coaxial. According to (12), we can replace the time derivative of elastic and inelastic Hencky strains appearing in (24) with any corotational rate in the form of (10). We particularly make use of the corresponding logarithmic spin tensors, i.e., $\boldsymbol{\Omega}^{log\text{-}e}$ and $\boldsymbol{\Omega}^{log\text{-}in}$, which according to (13) result in[8]:

$$\frac{\partial\psi^e}{\partial\bar{\boldsymbol{h}}^e} : \dot{\bar{\boldsymbol{h}}}^e = \frac{\partial\psi^e}{\partial\bar{\boldsymbol{h}}^e} : (\overset{\circ}{\bar{\boldsymbol{h}}}^e)^{log\text{-}e} = \frac{\partial\psi^e}{\partial\bar{\boldsymbol{h}}^e} : \bar{\boldsymbol{d}}^e, \tag{25}$$

and

$$\frac{\partial\psi^{in}}{\partial\bar{\boldsymbol{h}}^{in}} : \dot{\bar{\boldsymbol{h}}}^{in} = \frac{\partial\psi^{in}}{\partial\bar{\boldsymbol{h}}^{in}} : (\overset{\circ}{\bar{\boldsymbol{h}}}^{in})^{log\text{-}in} = \frac{\partial\psi^{in}}{\partial\bar{\boldsymbol{h}}^{in}} : \bar{\boldsymbol{d}}^{in}, \tag{26}$$

where superscripts "log-e" and "log-in" represent the corotational rate associated with the logarithmic spins during the elastic and inelastic deformations, $\overline{\boldsymbol{F}}^e$ and $\overline{\boldsymbol{F}}^{in}$, respectively.

Substituting (25) and (26) into (24), after some mathematical manipulations, we obtain:

$$\left(p - \frac{\partial\phi^e}{\partial\theta^e}\right)\dot{\theta}^e + \left(\boldsymbol{s} - \frac{\partial\psi^e}{\partial\bar{\boldsymbol{h}}^e}\right) : \bar{\boldsymbol{d}}^e + \left(p - \frac{\partial\phi^{in}}{\partial\theta^{in}}\right)\dot{\theta}^{in} + \left(\overline{\boldsymbol{F}}^{e^T}\boldsymbol{s}\overline{\boldsymbol{F}}^{e^{-T}} - \frac{\partial\psi^{in}}{\partial\bar{\boldsymbol{h}}^{in}}\right) : \bar{\boldsymbol{l}}^{in} - \left(\eta + \frac{\partial\psi^{in}}{\partial T}\right)\dot{T} \geqslant 0. \tag{27}$$

In deriving (27) we have used the symmetric property of both $\boldsymbol{s}$ and $\frac{\partial\psi^{in}}{\partial\bar{\boldsymbol{h}}^{in}}$ implying, respectively:

$$\boldsymbol{s} : \mathrm{sym}\left(\overline{\boldsymbol{F}}^e\bar{\boldsymbol{l}}^{in}\overline{\boldsymbol{F}}^{e^{-1}}\right) = \boldsymbol{s} : \left(\overline{\boldsymbol{F}}^e\bar{\boldsymbol{l}}^{in}\overline{\boldsymbol{F}}^{e^{-1}}\right) = \bar{\boldsymbol{l}}^{in} : \left(\overline{\boldsymbol{F}}^{e^T}\boldsymbol{s}\overline{\boldsymbol{F}}^{e^{-T}}\right), \tag{28}$$

and

$$\frac{\partial\psi^{in}}{\partial\bar{\boldsymbol{h}}^{in}} : \bar{\boldsymbol{d}}^{in} = \frac{\partial\psi^{in}}{\partial\bar{\boldsymbol{h}}^{in}} : \bar{\boldsymbol{l}}^{in}. \tag{29}$$

The inequality (27) must be fulfilled for arbitrary thermodynamic processes, i.e. for arbitrary $\dot{\theta}^e$, $\bar{\boldsymbol{d}}^e$, $\dot{\theta}^{in}$, $\bar{\boldsymbol{d}}^{in}$ and $\dot{T}$. For arbitrary choices of the variables $\dot{\theta}^e$, $\bar{\boldsymbol{d}}^e$ and $\dot{T}$, we may conclude[9] (Haupt, 2002; Ottosen and Ristinmaa, 2005):

$$p = \frac{\partial\phi^e}{\partial\theta^e}, \quad \boldsymbol{s} = \frac{\partial\psi^e}{\partial\bar{\boldsymbol{h}}^e}, \quad \eta = -\frac{\partial\psi^{in}}{\partial T}, \tag{30}$$

and the following simplified Clausius–Duhem inequality to guarantee the non-negativeness of the internal dissipation (required by the second law of thermodynamics):

$$\left(p - \frac{\partial\phi^{in}}{\partial\theta^{in}}\right)\dot{\theta}^{in} + \left(\overline{\boldsymbol{F}}^{e^T}\boldsymbol{s}\overline{\boldsymbol{F}}^{e^{-T}} - \frac{\partial\psi^{in}}{\partial\bar{\boldsymbol{h}}^{in}}\right) : \bar{\boldsymbol{l}}^{in} \geqslant 0. \tag{31}$$

[8] According to the work by Xiao et al. (1997), the logarithmic spin $\boldsymbol{\Omega}^{log}$ is introduced as

$$\boldsymbol{\Omega}^{log}(\boldsymbol{F}) = \boldsymbol{w} + \sum_{i,j=1,i\neq j}^{m}\left[\left(\frac{1+(b_i/b_j)}{1-(b_i/b_j)} + \frac{2}{\log(b_i/b_j)}\right)\boldsymbol{P}_i\boldsymbol{d}\boldsymbol{P}_j\right],$$

where $b_i = \lambda_i^2$ are the eigenvalues of the left Cauchy–Green deformation tensor and $\boldsymbol{P}_i$ are the eigenprojections subordinate to eigenvalues $\lambda_i > 0$. According to this relation, knowing the deformation gradient $\boldsymbol{F}(t)$, the logarithmic spin $\boldsymbol{\Omega}^{log}(\boldsymbol{F})$ can be computed. We now consider the multiplicative decomposition of the deformation gradient and introduce the logarithmic spins $\boldsymbol{\Omega}^{log\text{-}e}$ and $\boldsymbol{\Omega}^{log\text{-}in}$ as follows:

$$\boldsymbol{\Omega}^{log\text{-}e} = \boldsymbol{\Omega}^{log}(\overline{\boldsymbol{F}}^e) \quad \text{and} \quad \boldsymbol{\Omega}^{log\text{-}in} = \boldsymbol{\Omega}^{log}(\overline{\boldsymbol{F}}^{in}),$$

[9] In the work by Xiao et al. (2000), they use the hypoelastic constitutive model $\boldsymbol{d}^e = \overline{(\partial\Sigma/\partial\boldsymbol{\pi})}^{log\text{-}e}$, where Σ is a complementary hyperelastic potential and $\boldsymbol{\pi} = \boldsymbol{R}\boldsymbol{\Pi}\boldsymbol{R}^T$ is the Eulerian stress while $\boldsymbol{\Pi}$ is the work-conjugate stress measure of the Lagrangean logarithmic strain $\boldsymbol{H}$. However, the corresponding hypoelastic constitutive model of this work, when written in the framework of Xiao et al. (2000) work, takes the form $\boldsymbol{d}^e = \overline{(\partial\Sigma/\partial\boldsymbol{\pi})}^{log\text{-}e}$. It is noted that regarding the fact that $\boldsymbol{d}^e = \boldsymbol{h}^{e\,log\text{-}e}$, we can write $\boldsymbol{h}^{e\,log\text{-}e} = \overline{(\partial\Sigma/\partial\boldsymbol{\pi})}^{log\text{-}e}$ which can be integrated to yield $\boldsymbol{h}^e = \partial\Sigma/\partial\boldsymbol{\pi}$. This shows that, the hypoelastic form used in this work can be reduced to a hyperelastic constitutive model as observed in $(30)_{1,2}$.

Considering $(30)_2$ and the isotropic property of ψ^e, it can be shown that $\bar{\boldsymbol{F}}^{e^T}\boldsymbol{s}\bar{\boldsymbol{F}}^{e^{-T}}$ is a symmetric tensor (see Eq. (118) in the Appendix A). Therefore, Eq. (31) reads as

$$q\dot{\theta}^{in} + \boldsymbol{\alpha} : \bar{\boldsymbol{d}}^{in} \geqslant 0, \tag{32}$$

where the scalar and tensorial relative stresses, q and $\boldsymbol{\alpha}$, are defined as

$$\begin{aligned} q &= p - \frac{\partial \phi^{in}}{\partial \theta^{in}} = \frac{\partial \phi^{e}}{\partial \theta^{e}} - \frac{\partial \phi^{in}}{\partial \theta^{in}}, \\ \boldsymbol{\alpha} &= \boldsymbol{m} - \boldsymbol{x}, \end{aligned} \tag{33}$$

with

$$\boldsymbol{m} = \bar{\boldsymbol{F}}^{e^T}\boldsymbol{s}\bar{\boldsymbol{F}}^{e^{-T}}, \quad \boldsymbol{x} = \frac{\partial \psi^{in}}{\partial \bar{\boldsymbol{h}}^{in}}. \tag{34}$$

To satisfy the second law of thermodynamics (32), following Ottosen and Ristinmaa (2005), we introduce the convex potential $G(\boldsymbol{\alpha}, q)$ and define the following evolution equations:

$$\bar{\boldsymbol{d}}^{in} = \dot{\lambda}\frac{\partial G(\boldsymbol{\alpha}, q)}{\partial \boldsymbol{\alpha}} \quad \text{and} \quad \dot{\theta}^{in} = \dot{\lambda}\frac{\partial G(\boldsymbol{\alpha}, q)}{\partial q}, \tag{35}$$

where λ is the consistency parameter.

Moreover, we consider a yield or limit function as follows:

$$F = f(\boldsymbol{\alpha}, q) - R, \tag{36}$$

where the material parameter $R$is the elastic region radius.

Similarly to plasticity, the consistency parameter and the limit function (or yield function) satisfy the Kuhn–Tucker conditions:

$$F \leqslant 0, \quad \dot{\lambda} \geqslant 0, \quad \dot{\lambda}F = 0. \tag{37}$$

Accordingly, the finite strain, non-associative constitutive model can be summarized as

- Stress-like quantities:

$$p = \frac{\partial \phi^{e}}{\partial \theta^{e}}, \quad q = \frac{\partial \phi^{e}}{\partial \theta^{e}} - \frac{\partial \phi^{in}}{\partial \theta^{in}}, \quad \boldsymbol{s} = \frac{\partial \psi^{e}}{\partial \bar{\boldsymbol{h}}^{e}}, \quad \boldsymbol{m} = \bar{\boldsymbol{F}}^{e^T}\boldsymbol{s}\bar{\boldsymbol{F}}^{e^{-T}}, \quad \boldsymbol{x} = \frac{\partial \psi^{in}}{\partial \bar{\boldsymbol{h}}^{in}}, \quad \boldsymbol{\alpha} = \boldsymbol{m} - \boldsymbol{x}.$$

- Limit function:

$$F = f(\boldsymbol{\alpha}, q) - R.$$

- Potential function:

$$G = G(\boldsymbol{\alpha}, q).$$

- Evolution equations:

$$\bar{\boldsymbol{d}}^{in} = \dot{\lambda}\frac{\partial G(\boldsymbol{\alpha}, q)}{\partial \boldsymbol{\alpha}} \quad \text{and} \quad \dot{\theta}^{in} = \dot{\lambda}\frac{\partial G(\boldsymbol{\alpha}, q)}{\partial q}.$$

- Kuhn–Tucker conditions:

$$F \leqslant 0, \quad \dot{\lambda} \geqslant 0, \quad \dot{\lambda}F = 0.$$

3.2. Representation with respect to the reference configuration

In the previous section, using a multiplicative decomposition of the deformation gradient into elastic and inelastic parts, we derived a finite-strain constitutive model. But while $\boldsymbol{F}$and $\boldsymbol{F}^{in}$ are related to the reference configuration, $\boldsymbol{F}^{e}$ is defined with respect to an intermediate configuration. Accordingly, tensor $\boldsymbol{s}$ has been defined with respect to the current configuration, while tensors $\boldsymbol{m}$, $\boldsymbol{x}$, $\boldsymbol{\alpha}$ and $\bar{\boldsymbol{d}}^{in}$ have been defined with respect to the intermediate configuration. Thus, we recast all equations in terms of quantities defined with respect to the reference configuration, allowing to express all equations in a Lagrangian form.

As already stated, ψ^e depends on $\bar{\boldsymbol{h}}^e$ only through its invariants which are the same as those of $\bar{\boldsymbol{H}}^e$. Since $\bar{\boldsymbol{H}}^e = 1/2\log(\bar{\boldsymbol{C}}^e)$, it is clear that the invariants of $\bar{\boldsymbol{H}}^e$ can be expressed in terms of the invariants of $\bar{\boldsymbol{C}}^e$ which are equal to those of $\bar{\boldsymbol{U}}^{in^{-1}}\bar{\boldsymbol{C}}\bar{\boldsymbol{U}}^{in^{-1}}$. In fact, for the first invariant, the following identity holds:

$$I_{\bar{\boldsymbol{C}}^e} = \mathrm{tr}(\bar{\boldsymbol{C}}^e) = \mathrm{tr}\left(\bar{\boldsymbol{F}}^{in^{-T}}\bar{\boldsymbol{C}}\bar{\boldsymbol{F}}^{in^{-1}}\right) = \mathrm{tr}\left(\bar{\boldsymbol{U}}^{in^{-1}}\bar{\boldsymbol{C}}\bar{\boldsymbol{U}}^{in^{-1}}\right), \tag{38}$$

and similar relations hold for the second and the third invariants. Therefore, we conclude that the invariants of $\bar{\boldsymbol{h}}^e$ are equal to those of an elastic-like strain tensor $\mathcal{H}^e$ defined as

$$\mathcal{H}^e = \frac{1}{2}\log\left(\bar{\boldsymbol{U}}^{in^{-1}}\bar{\boldsymbol{C}}\bar{\boldsymbol{U}}^{in^{-1}}\right). \tag{39}$$

Considering the isotropic property of ψ^e and according to the representation theorem,[10] we now write:

$$\frac{\partial\psi^e}{\partial\bar{\boldsymbol{h}}^e} = \alpha_1\mathbf{1} + 2\alpha_2\bar{\boldsymbol{h}}^e + 4\alpha_3\bar{\boldsymbol{h}}^{e^2}, \tag{40}$$

where

$$\alpha_i = \alpha_i(I_{\bar{\boldsymbol{h}}^e}, II_{\bar{\boldsymbol{h}}^e}, III_{\bar{\boldsymbol{h}}^e}) = \alpha_i(I_{\mathcal{H}^e}, II_{\mathcal{H}^e}, III_{\mathcal{H}^e}). \tag{41}$$

It can be shown that (see Eq. (121) in the Appendix A):

$$\bar{\boldsymbol{h}}^e = \frac{1}{2}\bar{\boldsymbol{F}}^{-T}\log(\bar{\boldsymbol{C}}\bar{\boldsymbol{C}}^{in^{-1}})\bar{\boldsymbol{F}}^{T}. \tag{42}$$

We now substitute (42) into (40) and the result into $(30)_2$ which leads to:

$$\boldsymbol{s} = \bar{\boldsymbol{F}}^{-T}\boldsymbol{M}\bar{\boldsymbol{F}}^{T}, \tag{43}$$

where we have defined $\boldsymbol{M} = \alpha_1\mathbf{1} + \alpha_2\log(\bar{\boldsymbol{C}}\bar{\boldsymbol{C}}^{in^{-1}}) + \alpha_3(\log(\bar{\boldsymbol{C}}\bar{\boldsymbol{C}}^{in^{-1}}))^2$.

We now pull back the quantities $\boldsymbol{m}$ and $\boldsymbol{x}$ (which have been expressed with respect to the intermediate configuration) to the reference configuration. To this end, we use the identity $\bar{\boldsymbol{F}}^{e^T}\bar{\boldsymbol{h}}^e\bar{\boldsymbol{F}}^{e^{-T}} = \bar{\boldsymbol{H}}^e$ (see Eq. (117) in the Appendix A) as well as the following identity (see Eq. (122) in the Appendix A):

$$\bar{\boldsymbol{F}}^{in^T}\bar{\boldsymbol{H}}^e\bar{\boldsymbol{F}}^{in} = \frac{1}{2}\log\left(\bar{\boldsymbol{C}}\bar{\boldsymbol{C}}^{in^{-1}}\right)\bar{\boldsymbol{C}}^{in}, \tag{44}$$

and conclude:

$$\bar{\boldsymbol{F}}^{in^T}\boldsymbol{m}\bar{\boldsymbol{F}}^{in} = \boldsymbol{M}\bar{\boldsymbol{C}}^{in}. \tag{45}$$

We observe that tensor $\boldsymbol{M}$ is unsymmetric. In order to obtain a constitutive model in which all quantities are symmetric, we follow the recently proposed approach in Arghavani et al. (2010a) and utilize the following identity (see Eq. (124) in the Appendix A):

$$\log(\bar{\boldsymbol{C}}\bar{\boldsymbol{C}}^{in^{-1}}) = \bar{\boldsymbol{U}}^{in}\log\left(\bar{\boldsymbol{U}}^{in^{-1}}\bar{\boldsymbol{C}}\bar{\boldsymbol{U}}^{in^{-1}}\right)\bar{\boldsymbol{U}}^{in^{-1}}, \tag{46}$$

and express tensor $\boldsymbol{M}$ as

$$\boldsymbol{M} = \bar{\boldsymbol{U}}^{in}\boldsymbol{Q}\bar{\boldsymbol{U}}^{in^{-1}}, \tag{47}$$

where the symmetric tensor $\boldsymbol{Q}$is expressed as

$$\boldsymbol{Q} = \alpha_1\mathbf{1} + 2\alpha_2\mathcal{H}^e + 4\alpha_3\mathcal{H}^{e^2}. \tag{48}$$

Comparing (48) and (40), and considering (41), we use the representation theorem and express (48) as

$$\boldsymbol{Q} = \frac{\partial\psi^e(\mathcal{H}^e)}{\mathcal{H}^e}. \tag{49}$$

We now substitute (47) into (45), which yields:

$$\bar{\boldsymbol{F}}^{in^T}\boldsymbol{m}\bar{\boldsymbol{F}}^{in} = \bar{\boldsymbol{U}}^{in}\boldsymbol{Q}\bar{\boldsymbol{U}}^{in}. \tag{50}$$

Using the isotropic property of ψ^{in}, following a similar approach, we obtain:

$$\boldsymbol{x} = \frac{\partial\psi^{in}}{\partial\bar{\boldsymbol{h}}^{in}} = \beta_1\mathbf{1} + \beta_2\bar{\boldsymbol{h}}^{in} + \beta_3\bar{\boldsymbol{h}}^{in^2}, \tag{51}$$

where

$$\beta_i = \beta_i(I_{\bar{\boldsymbol{h}}^{in}}, II_{\bar{\boldsymbol{h}}^{in}}, III_{\bar{\boldsymbol{h}}^{in}}, T) = \beta_i(I_{\bar{\boldsymbol{H}}^{in}}, II_{\bar{\boldsymbol{H}}^{in}}, III_{\bar{\boldsymbol{H}}^{in}}, T). \tag{52}$$

[10] Representation theorem: A tensor function $\boldsymbol{D} = f(\boldsymbol{A})$ is isotropic if and only if it has a representation of the form $\boldsymbol{D} = f(\boldsymbol{A}) = \phi_0\mathbf{1} + \phi_1\boldsymbol{A} + \phi_2\boldsymbol{A}^2 + \cdots + \phi_{n-1}\boldsymbol{A}^{n-1}$ where the ϕ_k are invariants of $\boldsymbol{A}$ and hence can be expressed as functions $\phi_k = \phi_k(I_1,\ldots,I_n)$ of the principal invariants of $\boldsymbol{A}$ while n denotes the order of tensor $\boldsymbol{A}$. In the case when $n = 3$ the representation theorem reads $\boldsymbol{D} = f(\boldsymbol{A}) = \phi_0\mathbf{1} + \phi_1\boldsymbol{A} + \phi_2\boldsymbol{A}^2$ (Truesdell and Noll, 1965; Ogden, 1984; Ottosen and Ristinmaa, 2005).

We now use the identity $\overline{\boldsymbol{F}}^{in^T}\bar{\boldsymbol{h}}^{in}\overline{\boldsymbol{F}}^{in}=\overline{\boldsymbol{H}}^{in}\overline{\boldsymbol{C}}^{in}$ to obtain:

$$\overline{\boldsymbol{F}}^{in^T}\boldsymbol{\varkappa}\overline{\boldsymbol{F}}^{in}=\boldsymbol{X}\overline{\boldsymbol{C}}^{in}, \tag{53}$$

where

$$\boldsymbol{X}=\beta_1\mathbf{1}+\beta_2\overline{\boldsymbol{H}}^{in}+\beta_3\overline{\boldsymbol{H}}^{in^2}. \tag{54}$$

Similarly, comparing (51) and (54) and considering (52), we can express (54) as

$$\boldsymbol{X}=\frac{\partial\psi^{in}(\overline{\boldsymbol{H}}^{in})}{\partial\overline{\boldsymbol{H}}^{in}}. \tag{55}$$

Since $\boldsymbol{X}$ and $\overline{\boldsymbol{U}}^{in}$ are coaxial, the following identity holds:

$$\boldsymbol{X}=\overline{\boldsymbol{U}}^{in}\boldsymbol{X}\overline{\boldsymbol{U}}^{in^{-1}}. \tag{56}$$

Substituting (56) into (53), we obtain:

$$\overline{\boldsymbol{F}}^{in^T}\boldsymbol{\varkappa}\overline{\boldsymbol{F}}^{in}=\overline{\boldsymbol{U}}^{in}\boldsymbol{X}\overline{\boldsymbol{U}}^{in}. \tag{57}$$

Combining (50) and (57), we finally conclude:

$$\overline{\boldsymbol{F}}^{in^T}\boldsymbol{\alpha}\overline{\boldsymbol{F}}^{in}=\overline{\boldsymbol{F}}^{in^T}(\boldsymbol{m}-\boldsymbol{\varkappa})\overline{\boldsymbol{F}}^{in}=\overline{\boldsymbol{U}}^{in}\boldsymbol{Z}\overline{\boldsymbol{U}}^{in}, \tag{58}$$

where

$$\boldsymbol{Z}=\boldsymbol{Q}-\boldsymbol{X}. \tag{59}$$

Using (58), we obtain:

$$\overline{\boldsymbol{F}}^{in^T}\boldsymbol{\alpha}^n\overline{\boldsymbol{F}}^{in}=\overline{\boldsymbol{U}}^{in}\boldsymbol{Z}^n\overline{\boldsymbol{U}}^{in}\quad\text{and}\quad \mathrm{tr}(\boldsymbol{\alpha}^n)=\mathrm{tr}(\boldsymbol{Z}^n), \tag{60}$$

where n is a non-negative integer number. Eq. $(60)_2$ means that the invariants of $\boldsymbol{\alpha}$ and $\boldsymbol{Z}$ are the same.

We now assume $G(\boldsymbol{\alpha},q)$ and $F(\boldsymbol{\alpha},q)$ to be isotropic functions of $\boldsymbol{\alpha}$ which means that they are expressed only in terms of the invariants of $\boldsymbol{\alpha}$ which are equal to those of $\boldsymbol{Z}$. Therefore, we present the Lagrangian form of the potential and limit functions, respectively, as follows:

$$G=G(\boldsymbol{Z},q)\quad\text{and}\quad F=f(\boldsymbol{Z},q)-R. \tag{61}$$

In order to obtain the evolution equation in a Lagrangian form, we use relation $\dot{\overline{\boldsymbol{C}}}^{in}=2\overline{\boldsymbol{F}}^{in^T}\bar{\boldsymbol{d}}^{in}\overline{\boldsymbol{F}}^{in}$ and (35) to obtain:

$$\dot{\overline{\boldsymbol{C}}}^{in}=2\dot{\lambda}\overline{\boldsymbol{F}}^{in^T}\frac{\partial G(\boldsymbol{\alpha},q)}{\partial\boldsymbol{\alpha}}\overline{\boldsymbol{F}}^{in}. \tag{62}$$

Considering the isotropic property of $G(\boldsymbol{\alpha},q)$, the following identity holds (see Eq. (128) in the Appendix A):

$$\overline{\boldsymbol{F}}^{in^T}\frac{\partial G(\boldsymbol{\alpha},q)}{\partial\boldsymbol{\alpha}}\overline{\boldsymbol{F}}^{in}=\overline{\boldsymbol{U}}^{in}\frac{\partial G(\boldsymbol{Z},q)}{\partial\boldsymbol{Z}}\overline{\boldsymbol{U}}^{in}. \tag{63}$$

Finally, substituting (63) into (62), we obtain the Lagrangian form of the tensorial evolution equation as follows:

$$\dot{\overline{\boldsymbol{C}}}^{in}=2\dot{\lambda}\overline{\boldsymbol{U}}^{in}\frac{\partial G(\boldsymbol{Z},q)}{\partial\boldsymbol{Z}}\overline{\boldsymbol{U}}^{in}. \tag{64}$$

Moreover, the scalar internal variable evolution is stated as

$$\dot{\theta}^{in}=\dot{\lambda}\frac{\partial G(\boldsymbol{Z},q)}{\partial q}. \tag{65}$$

The second Piola–Kirchhoff stress tensor $\boldsymbol{S}$ is obtained from the Kirchhoff stress tensor as

$$\boldsymbol{S}=\boldsymbol{F}^{-1}\boldsymbol{\tau}\boldsymbol{F}^{-T}. \tag{66}$$

Substituting (17) and $\boldsymbol{\tau}=\boldsymbol{s}+p\mathbf{1}$ into (66) yields:

$$\boldsymbol{S}=J^{-2/3}\left(p\overline{\boldsymbol{C}}^{-1}+\overline{\boldsymbol{F}}^{-1}\boldsymbol{s}\overline{\boldsymbol{F}}^{-T}\right). \tag{67}$$

Substituting $(30)_1$ and (43) into (67), we obtain:

$$\boldsymbol{S}=J^{-2/3}\left(\acute{\phi}^e\overline{\boldsymbol{C}}^{-1}+\overline{\boldsymbol{C}}^{-1}\boldsymbol{M}\right), \tag{68}$$

where, $\acute{\phi}^e=\partial\phi^e/\partial\theta^e$.

We now substitute (47) into (68) and obtain the second Piola–Kirchhoff stress tensor as follows[11]:

$$\boldsymbol{S} = J^{-2/3}\overline{\boldsymbol{C}}^{-1}\left(\acute{\phi}^{e}\boldsymbol{1} + \overline{\boldsymbol{U}}^{in}\boldsymbol{Q}\overline{\boldsymbol{U}}^{in^{-1}}\right). \tag{69}$$

We finally summarizes the time-continuous finite-strain constitutive model, written only in terms of Lagrangian quantities in Table 1.

It is interesting that the proposed finite strain and the corresponding small strain (when the proposed model is linearized) constitutive models have similar forms, thanks to the Hencky strain. In particular, when linearized, the elastic-like strain tensor $\mathcal{H}^{e}$ is reduced to small-strain elastic strain tensor, i.e.

$$\mathcal{H}^{e} \simeq \boldsymbol{\varepsilon} - \boldsymbol{\varepsilon}^{in} + \text{higher order terms} \simeq \boldsymbol{\varepsilon}^{e}, \tag{70}$$

where $\boldsymbol{\varepsilon}$, $\boldsymbol{\varepsilon}^{e}$ and $\boldsymbol{\varepsilon}^{in}$ are, respectively, the total, elastic and inelastic small strain tensors. Eq. (70) makes clear the reason for choosing the name "elastic-like strain tensor" for $\mathcal{H}^{e}$.

4. The proposed constitutive model in the time-discrete frame

In this section, we investigate the time integration of the constitutive model derived in Section 3 with the final goal of using it within a finite element program. The main task is to apply an appropriate numerical time integration scheme to the evolution equation of the internal variables. In general, implicit schemes are preferred because of their stability at larger time step sizes.

We treat the nonlinear problem described in Section 3 as an implicit time-discrete deformation-driven problem. Accordingly, we subdivide the time interval of interest $[0,t]$ in sub-increments and we solve the evolution problem over the generic interval $[t_n,t_{n+1}]$ with $t_{n+1} > t_n$. To simplify the notation, we indicate with the subscript n a quantity evaluated at time t_n, and with no subscript a quantity evaluated at time t_{n+1}. Assuming to know the solution and the deformation gradient $\boldsymbol{F}_n$ at time t_n as well as the deformation gradient $\boldsymbol{F}$ at time t_{n+1}, the internal variables (and the stress tensor) should be updated from the deformation history.

Since, the constitutive model is in terms of Lagrangian quantities, from now on, we consider as deformation driver the right Cauchy–Green deformation tensor (instead of the deformation gradient), assuming $\overline{\boldsymbol{C}}$ and θ are given (control variables).

4.1. Time integration

We use a backward-Euler integration scheme for the scalar internal variable evolution Eq. (65) and obtain:

$$\theta^{in} = \theta^{in}_{n} + \Delta\lambda\frac{\partial G(\boldsymbol{Z},q)}{\partial q}, \tag{71}$$

where $\Delta\lambda = \lambda - \lambda_n$.

However, time integration of the tensorial internal variable $\overline{\boldsymbol{C}}^{in}$ is not straightforward and the time-discrete form should satisfy the incompressibility constraint $\det(\overline{\boldsymbol{C}}^{in}) = 1$.

To this end, exponential-based integration schemes are frequently applied to problems in plasticity and isotropic inelasticity (Eterovic and Bathe, 1990; Miehe, 1996). The use of the exponential mapping enables to exactly conserve the inelastic volume. Thus, it allows larger time step sizes than any other first-order accurate integration scheme.

We now consider the following form of the evolution equation and investigate its time-discrete form:

$$\dot{\overline{\boldsymbol{C}}}^{in} = \dot{\lambda}\boldsymbol{A} \quad \text{and} \quad \det(\overline{\boldsymbol{C}}^{in}) = 1. \tag{72}$$

Applying the exponential mapping scheme to the evolution Eq. (72), Reese and Christ (2008) have proposed the following time-discrete form which has also been used in several works (Christ and Reese, 2009; Evangelista et al., 2009; Vladimirov et al., 2008, 2010; Arghavani et al., 2010b):

$$-\overline{\boldsymbol{C}}^{in^{-1}}_{n} + \overline{\boldsymbol{U}}^{in^{-1}}\exp\left(\Delta\lambda\overline{\boldsymbol{U}}^{in^{-1}}\boldsymbol{A}\overline{\boldsymbol{U}}^{in^{-1}}\right)\overline{\boldsymbol{U}}^{in^{-1}} = \boldsymbol{0}. \tag{73}$$

Recently Arghavani et al. (2010b) have proposed an alternative form of the time-discrete evolution Eq. (73) through the following logarithmic mapping which is more robust and efficient when compared with (73):

$$-\overline{\boldsymbol{U}}^{in}\log\left(\overline{\boldsymbol{U}}^{in}\overline{\boldsymbol{C}}^{in^{-1}}_{n}\overline{\boldsymbol{U}}^{in}\right)\overline{\boldsymbol{U}}^{in} + \Delta\lambda\boldsymbol{A} = \boldsymbol{0}. \tag{74}$$

In Table 2, we have summarized the time-integration algorithms (Arghavani et al., 2010b).

[11] According to Eq. (69), the so-called Mandel stress is $\boldsymbol{CS} = \acute{\phi}^{e}\boldsymbol{1} + \overline{\boldsymbol{U}}^{in}\boldsymbol{Q}\overline{\boldsymbol{U}}^{in^{-1}} = \overline{\boldsymbol{U}}^{in}(\acute{\phi}^{e}\boldsymbol{1} + \boldsymbol{Q})\overline{\boldsymbol{U}}^{in^{-1}}$ which is, in general, an asymmetric tensor.

Table 1
Finite-strain kinematic hardening constitutive model in the time-continuous frame.

External variables: $\overline{\boldsymbol{C}},\ \theta,\ T$
Internal variables: $\overline{\boldsymbol{U}}^{in},\ \theta^{in}$
Stress quantities: $\boldsymbol{Q}=\frac{\partial\psi^{e}(\mathscr{H}^{e})}{\partial\mathscr{H}^{e}}\quad \boldsymbol{X}=\frac{\partial\psi^{in}(\overline{\boldsymbol{H}}^{in})}{\partial\overline{\boldsymbol{H}}^{in}}\quad \boldsymbol{Z}=\boldsymbol{Q}-\boldsymbol{X}\quad q=\acute{\phi}^{e}-\acute{\phi}^{in}$ with
$\overline{\boldsymbol{H}}^{in}=\log(\overline{\boldsymbol{U}}^{in}),\quad \mathscr{H}^{e}=\frac{1}{2}\log\left(\overline{\boldsymbol{U}}^{in^{-1}}\overline{\boldsymbol{C}}\overline{\boldsymbol{U}}^{in^{-1}}\right)$ and $\acute{\phi}^{e}=\partial\phi^{e}/\partial\theta^{e},\quad \acute{\phi}^{in}=\partial\phi^{in}/\partial\theta^{in}$ and $\theta^{e}=\theta-\theta^{in}$,
Limit function: $F=f(\boldsymbol{Z},q)-R$
Potential function: $G=G(\boldsymbol{Z},q)$
Evolution equations: $\dot{\overline{\boldsymbol{C}}}^{in}=2\dot{\lambda}\overline{\boldsymbol{U}}^{in}\frac{\partial G(\boldsymbol{Z},q)}{\partial\boldsymbol{Z}}\overline{\boldsymbol{U}}^{in}$ and $\dot{\theta}^{in}=\dot{\lambda}\frac{\partial G(\boldsymbol{Z},q)}{\partial q}$
Kuhn–Tucker conditions: $F\leqslant 0,\ \dot{\lambda}\geqslant 0,\ \dot{\lambda}F=0$

Table 2
Time integration algorithms: exponential and logarithmic mappings (Arghavani et al., 2010b).

Time-continuous form: $\dot{\overline{\boldsymbol{C}}}^{in}=\dot{\lambda}\boldsymbol{A},\quad \det(\overline{\boldsymbol{C}}^{in})=1$
Time-discrete form based on exponential mapping: $-\overline{\boldsymbol{C}}_{n}^{in^{-1}}+\overline{\boldsymbol{U}}^{in^{-1}}\exp(\Delta\lambda\overline{\boldsymbol{U}}^{in^{-1}}\boldsymbol{A}\overline{\boldsymbol{U}}^{in^{-1}})\overline{\boldsymbol{U}}^{in^{-1}}=\boldsymbol{0}$
Time-discrete form based on logarithmic mapping: $-\overline{\boldsymbol{U}}^{in}\log(\overline{\boldsymbol{U}}^{in}\overline{\boldsymbol{C}}_{n}^{in^{-1}}\overline{\boldsymbol{U}}^{in})\overline{\boldsymbol{U}}^{in}+\Delta\lambda\boldsymbol{A}=\boldsymbol{0}$

Comparing (72) and (64), we conclude:

$$\boldsymbol{A}=2\overline{\boldsymbol{U}}^{in}\frac{\partial G(\boldsymbol{Z},q)}{\partial\boldsymbol{Z}}\overline{\boldsymbol{U}}^{in}. \tag{75}$$

We now substitute (75) into (73) to obtain the time-discrete form of the evolution Eq. (64) based on the exponential mapping:

$$-\overline{\boldsymbol{C}}_{n}^{in^{-1}}+\overline{\boldsymbol{U}}^{in^{-1}}\exp\left(2\Delta\lambda\frac{\partial G(\boldsymbol{Z},q)}{\partial\boldsymbol{Z}}\right)\overline{\boldsymbol{U}}^{in^{-1}}=\boldsymbol{0}. \tag{76}$$

Substituting (75) into (74), we obtain:

$$-\overline{\boldsymbol{U}}^{in}\log\left(\overline{\boldsymbol{U}}^{in}\overline{\boldsymbol{C}}_{n}^{in^{-1}}\overline{\boldsymbol{U}}^{in}\right)\overline{\boldsymbol{U}}^{in}+2\Delta\lambda\overline{\boldsymbol{U}}^{in}\frac{\partial G(\boldsymbol{Z},q)}{\partial\boldsymbol{Z}}\overline{\boldsymbol{U}}^{in}=\boldsymbol{0}. \tag{77}$$

We now, left- and right-multiply (77) by $\overline{\boldsymbol{U}}^{in^{-1}}$ and obtain the time-discrete form of the evolution equation, based on the logarithmic mapping as follows:

$$-\log\left(\overline{\boldsymbol{U}}^{in}\overline{\boldsymbol{C}}_{n}^{in^{-1}}\overline{\boldsymbol{U}}^{in}\right)+2\Delta\lambda\frac{\partial G(\boldsymbol{Z},q)}{\partial\boldsymbol{Z}}=\boldsymbol{0}. \tag{78}$$

We finally remark that, since $\boldsymbol{Z}$ contains logarithmic terms, (78) includes only logarithmic terms, while in (76) an exponential term exists. The time-discrete evolution Eqs. (71) and (78) together with the limit (yield) condition (61) construct a system of nonlinear equations, i.e.

$$\begin{cases}-\log\left(\overline{\boldsymbol{U}}^{in}\overline{\boldsymbol{C}}_{n}^{in^{-1}}\overline{\boldsymbol{U}}^{in}\right)+2\Delta\lambda\frac{\partial G(\boldsymbol{Z},q)}{\partial\boldsymbol{Z}}=\boldsymbol{0},\\ -\theta^{in}+\theta_{n}^{in}+\Delta\lambda\frac{\partial G(\boldsymbol{Z},q)}{\partial q}=0,\\ F(\boldsymbol{Z},q)=0,\end{cases} \tag{79}$$

Solution of system of Eq. (79) is, in general, approached through a straightforward Newton–Raphson method to find $\overline{\boldsymbol{U}}^{in},\ \theta^{in}$ and $\Delta\lambda$.

5. Application to shape memory alloy modeling

We now particularize the inelastic model and the corresponding solution algorithm presented in Sections 3 and 4 to a particular class of materials known as shape memory alloys.

Intelligent, smart or functional materials exhibit special properties that make them a suitable choice for industrial applications in many branches of engineering. Among different types of smart materials, shape memory alloys (SMAs) have unique features known as pseudo-elasticity, one-way and two-way shape memory effects (Otsuka and Wayman, 1998; Duerig et al., 1990). The origin of SMA material features is a reversible thermo-elastic martensitic phase transformation between a high symmetry, austenitic phase and a low symmetry, martensitic phase.

When the transformation is driven by a temperature decrease, martensite variants compensate each other, resulting in no macroscopic deformation. However, when the transformation is driven by the application of a load, specific martensite variants, favorable to the applied stress, are preferentially formed, exhibiting a macroscopic shape change in the direction of the

applied stress. Upon unloading or heating, this shape change disappears through the reversible conversion of the martensite variants into the parent phase (Otsuka and Wayman, 1998; Funakubo, 1987).

During the forward transformation, under zero load, austenite begins to transform to twinned martensite at the martensitic start temperature (M_s) and completes transformation to martensite at the martensitic finish temperature (M_f). Similarly, during heating, the reverse transformation initiates at the austenitic start temperature (A_s) and the transformation is completed at the austenitic finish temperature (A_f). Applying a stress at a temperature above A_f, SMAs exhibit pseudo-elastic behavior with a full recovery of inelastic strain upon unloading, while at a temperature below M_s, the material presents the shape memory effect with permanent inelastic strains upon unloading which may be recovered by heating.

In most applications, SMAs experience complicated multi-axial loadings, typically undergoing very large rotations and moderate strains (i.e., in the range of 10–15% for polycrystals Shaw, 2000). For example, with reference to biomedical applications, stent structures are usually designed to significantly reduce their diameter during the insertion into a catheter; thereby, large rotations combined with moderate strains occur.

The so-called variant reorientation has been observed to be the main phenomenon in non-proportional loadings of SMAs (Lim and McDowell, 1999; Sittner et al., 1995; Helm, 2001, 2002; Bouvet et al., 2002; Grabe and Bruhns, 2009). Recently, Grabe and Bruhns (2009) have conducted several multi-axial experiments on polycrystalline NiTi within a wide temperature range, showing the strong nonlinearity as well as the path dependencies of the response and highlighting the presence of reorientation processes for complex loading paths.

These experimental observations, as well as situations experienced by SMAs in real engineering applications, call for the development of a 3D SMA constitutive model, taking into account both finite strain and variant reorientation under general loading conditions (multi-axial non-proportional loadings).

Up to now several 3D SMA constitutive models have been proposed in the small deformation regime (Raniecki et al., 1992, 1994; Leclercq and Lexcellent, 1996; Bekker and Brinson, 1997; Raniecki and Lexcellent, 1998; Souza et al., 1998; Qidwai and Lagoudas, 2000; Helm and Haupt, 2003; Auricchio et al., 2003; Bouvet et al., 2004; Lagoudas and Entchev, 2004; Auricchio et al., 2007; Popov and Lagoudas, 2007; Panico and Brinson, 2007; Thiebaud et al., 2007; Moumni et al., 2008; Arghavani et al., 2010c).

Finite strain SMA constitutive models available in the literature have been mainly developed by extending small strain constitutive models. The approach in most of the cases is based on the multiplicative decomposition of the deformation gradient into an elastic and an inelastic or transformation part (Auricchio and Taylor, 1997; Helm, 2001; Auricchio, 2001; Pethö, 2001; Ziolkowski, 2007; Helm, 2007; Reese and Christ, 2008; Christ and Reese, 2009; Evangelista et al., 2009; Thamburaja, 2010; Arghavani et al., 2010d,), although there are some models in the literature which have utilized an additive decomposition of the strain rate tensor into an elastic and an inelastic part (Müller and Bruhns, 2004, 2006). Moreover, some finite strain non-phenomenological models have been proposed in the literature (see e.g., Patoor et al., 1996; Thamburaja and Anand, 2001, 2005; Pan et al., 2007a,b; Stein and Sagar, 2008 among others).

In the constitutive models based on the multiplicative decomposition of the deformation gradient, Green–Lagrange strain has been used as a strain measure and in most cases the obtained constitutive models are in a Lagrangian form. In the approaches based on the use of Green–Lagrange strain, one critical point is introducing a relation between martensite volume fraction, z, and the norm of the Green–Lagrange strain measure[12] (since $0 \leqslant z \leqslant 1$ it can be considered as a constraint on the inelastic strain). While the martensite fraction is a physical quantity, the Green–Lagrange strain is not a physical measure of strain. Considering this point, the proposed finite strain model which is based on the true strain is preferred.

On the other hand, in the constitutive models in which logarithmic strain is used as a (physical) strain measure, the additive decomposition of the strain rate tensor is adopted and the final form of the constitutive equations are Eulerian and objective rates should be used. For example, Müller and Bruhns (2004, 2006) have used a corotational rate associated to the logarithmic spin in their formulations.

In this work, we use the logarithmic strain as a physical measure of strain and based on the multiplicative decomposition of the deformation gradient we present a constitutive model in a Lagrangian form. Moreover, we develop a finite-strain SMA model by extending a small-strain constitutive model proposed by Souza et al. (1998), its capability has been shown in several works (Auricchio and Petrini, 2002, 2004a,b; Arghavani et al., 2010c). The small-strain model is capable in predicting both super-elasticity and shape memory effect as well as variant reorientation under non-proportional loading; it also has a suitable form which makes it possible to develop a robust integration algorithm as well as a successful computational tool (Arghavani et al., 2010b).

To this end, we use the proposed constitutive model in Section 3 (summarized in Table 1) and assuming appropriate form for strain energy functions in Section 5.1, we propose a Hencky-based finite strain constitutive model for shape memory alloys. In Section 5.2, we present a non-singular, continuous definition for the model variables, avoiding extensively-used regularization schemes. Section 5.3 describes the solution algorithm followed by defining a *Nucleation–Completion* condition (Arghavani et al., 2010b) in Section 5.4 and consistent tangent construction in Section 5.5. Finally in Section 6, implementing the proposed SMA constitutive model as well as the solution algorithm into a user defined subroutine UMAT in the nonlinear finite element software ABAQUS/Standard, we solve several boundary value problems.

[12] It has been defined in several works (Arghavani et al., 2010d; Reese and Christ, 2008; Christ and Reese, 2009; Helm and Haupt, 2003; Evangelista et al., 2009) as $z = \frac{\|\boldsymbol{E}^{in}\|}{e_L}$, where e_L is a material parameter related to the maximum transformation strain.

5.1. Strain energy function forms

We now assume the following forms for the elastic strain energy functions[13]:

$$\phi^e(\theta^e) = \frac{1}{2}K\theta^{e^2}, \quad \psi^e(\bar{\boldsymbol{h}}^e) = \mu \, \|\bar{\boldsymbol{h}}^e\|^2, \tag{80}$$

where K and μ are the material parameters.

Since experimental evidence indicates that phase transformation-induced deformations in SMAs are nearly isochoric, we have to impose $\det(\boldsymbol{F}^{in}) = 1$, which after taking the time derivative results in:

$$\mathrm{tr}(\boldsymbol{d}^{in}) = 0. \tag{81}$$

Therefore, $J^{in} = 1$ (or $\theta^{in} = 0$) is a known quantity. For this reason, without loss of generality, we can assume $\phi^{in}(\theta^{in}) = 0$. In the following, for simplicity, we denote all inelastic quantities without a bar symbol.

In order to describe SMAs behavior, we use the following form for ψ^{in} and we denote it by ψ^t to clarify it as the transformation strain energy function (Souza et al., 1998; Arghavani et al., 2010b):

$$\psi^{in} = \psi^t(\boldsymbol{h}^t, T) = \tau_M\|\boldsymbol{h}^t\| + \frac{1}{2}h_k\|\boldsymbol{h}^t\|^2 + \mathcal{I}_{\varepsilon_L}(\|\boldsymbol{h}^t\|), \tag{82}$$

where $\tau_M = \beta\,\langle T - T_0\rangle$ and β, T_0 as well as the kinematic hardening parameter h_k are material parameters. Also, the Macaulay brackets calculate the positive part of the argument, i.e. $\langle x\rangle = (x + |x|)/2$and the norm operator is defined as $\|\boldsymbol{A}\| = \sqrt{\boldsymbol{A} : \boldsymbol{A}}$.

Moreover, in Eq. (82) we use the indicator function $\mathcal{I}_{\varepsilon_L}$ defined as

$$\mathcal{I}_{\varepsilon_L}(\|\boldsymbol{h}^t\|) = \begin{cases} 0 & \text{if } \|\boldsymbol{h}^t\| \leqslant \varepsilon_L, \\ +\infty & \text{otherwise}, \end{cases} \tag{83}$$

to satisfy the constraint on the transformation strain norm (i.e., $\|\boldsymbol{h}^t\| \leqslant \varepsilon_L$). The material parameter ε_L is the maximum transformation strain norm in a uni-axial test.

We assume an associated case ($F = G$) and consider a von-Mises type limit (yield) function as[14]

$$F(\boldsymbol{Z}, q) = \|\boldsymbol{Z}\| - R. \tag{84}$$

We now compute the strain energy functions derivative as follows:

$$\acute{\phi}^e = \frac{\partial\phi^e}{\partial\theta^e} = K\theta^e, \quad \frac{\partial\psi^e}{\partial\bar{\boldsymbol{h}}^e} = 2\mu\bar{\boldsymbol{h}}^e, \tag{85}$$

which yields:

$$\alpha_1 = 0, \quad \alpha_2 = \mu, \quad \alpha_3 = 0, \tag{86}$$

and accordingly:

$$\boldsymbol{Q} = \mu\log\left(\boldsymbol{U}^{in^{-1}}\overline{\boldsymbol{C}}\boldsymbol{U}^{in^{-1}}\right) = 2\mu\mathcal{H}^e. \tag{87}$$

In a similar approach, we obtain:

$$\frac{\partial\psi^t}{\partial\boldsymbol{h}^t} = h_k\boldsymbol{h}^t + (\tau_M(T) + \gamma)\frac{\boldsymbol{h}^t}{\|\boldsymbol{h}^t\|}. \tag{88}$$

The positive variable γ results from the indicator function subdifferential $\partial\mathcal{I}_{\varepsilon_L}(\boldsymbol{h}^t)$ and it is defined as

$$\begin{cases} \gamma \geqslant 0 & \text{if } \|\boldsymbol{H}^t\| = \varepsilon_L, \\ \gamma = 0 & \text{if } \|\boldsymbol{H}^t\| < \varepsilon_L. \end{cases} \tag{89}$$

We then conclude:

$$\beta_1 = 0, \quad \beta_2 = h_k + \frac{\tau_M(T) + \gamma}{\|\boldsymbol{H}^t\|}, \quad \beta_3 = 0. \tag{90}$$

[13] This is a Hookean-type strain energy function in terms of Hencky strain. It is also known as Hencky model in the literature (see e.g., Xiao and Chen (2002)).

[14] For a kinematic hardening plasticity, we can assume a quadratic form for ψ^{in}, denoted by ψ^p:

$$\psi^{in} = \psi^p(\boldsymbol{h}^p, T) = \frac{1}{2}h_k\|\boldsymbol{h}^p\|^2,$$

Comparing the above equation and (82), we can conclude that a SMA constitutive model is reduced to a kinematic hardening plasticity model, when $\tau_M(T) = 0$ (or $T < T_0$) and $\varepsilon_L \to \infty$. To this reason, The proposed SMA constitutive model is capable to describe associated von-Mises type kinematic hardening plasticity.

In Eqs. (89) and (90), we have also used the property of $\|\boldsymbol{h}^t\| = \|\boldsymbol{H}^t\|$. Substituting (90) into (54), we obtain:

$$\boldsymbol{X} = h_k \boldsymbol{H}^t + (\tau_M(T) + \gamma)\boldsymbol{N}, \tag{91}$$

where $\boldsymbol{N} = \boldsymbol{H}^t/\|\boldsymbol{H}^t\|$.

5.2. Presentation of a well-defined form

We note that the variable $\boldsymbol{N}$ is not defined for the case of vanishing transformation strain. This is an issue in most of the SMA constitutive models (Evangelista et al., 2009; Helm and Haupt, 2003; Reese and Christ, 2008; Panico and Brinson, 2007) and a regularization scheme is extensively used in the literature to overcome this problem. This issue has recently been investigated by Arghavani et al. (2010c) and Arghavani et al. (2010b) in the small-strain and the finite-strain regime, respectively. They revised $\boldsymbol{N}$ as a well-defined, non-singular and continuous variable. Moreover, in Arghavani et al. (2010b) it is shown that using a regularization scheme increases solution time and consequently decreases computational efficiency. In fact, in a regularized scheme, most of the elastic behavior of the austenitic phase is considered as a phase transforming case for which a nonlinear system has to be solved. This can have a remarkable effect on the solution time for structures like stents in which considerable part of the structure remains elastic.

In the following, motivated by the work by Arghavani et al. (2010b), we suggest to avoid a regularized form for $\|\boldsymbol{H}^t\|$ and to deal with the case of vanishing transformation strain through a careful analytical study of the limiting conditions. We start investigating a condition in which $\boldsymbol{H}^t$ starts to evolve from a zero value (indicated in the following as *Nucleation*), i.e., $\boldsymbol{H}^t = \boldsymbol{0}$ with $\|\overline{\boldsymbol{H}^t}\| > 0$. Substituting $\boldsymbol{U}^t = \boldsymbol{1}$ into (59)[15] we conclude that $\boldsymbol{Z} = \boldsymbol{Q}_e$. We now consider the evolution equation which yields:

$$\dot{\boldsymbol{C}}^t = 2\dot{\lambda}\frac{\boldsymbol{Q}_e}{\|\boldsymbol{Q}_e\|}, \tag{92}$$

where $\boldsymbol{Q}_e = \mu \log(\overline{\boldsymbol{C}}) = 2\mu\overline{\boldsymbol{H}}$ is obtained from (87) substituting $\boldsymbol{1}$ in place of $\boldsymbol{U}^t$. According to (92), the transformation strain, $\boldsymbol{H}^t = \frac{1}{2}\log(\boldsymbol{C}^t) \simeq \frac{1}{2}(\boldsymbol{C}^t - \boldsymbol{1})$, nucleates in the $\boldsymbol{Q}_e$ direction.

We now investigate the case when transformation strain vanishes from a nonzero value (indicated in the following as *Completion*), i.e., $\boldsymbol{H}^t = \boldsymbol{0}$ ($\boldsymbol{U}^t = \boldsymbol{1}$) with $\|\overline{\boldsymbol{H}^t}\| < 0$. Since $\|\boldsymbol{H}^t\| = 0$, we conclude that adopting any arbitrary direction $\boldsymbol{N}$ leads to $\boldsymbol{H}^t = \boldsymbol{0}$. As stated in Arghavani et al. (2010c) (for a small-strain case), we select this direction as the $\boldsymbol{Q}_e$ direction which also guarantees continuity. Therefore, we revise the variable $\boldsymbol{N}$ in the following form:

$$\boldsymbol{N} = \begin{cases} \frac{\boldsymbol{Q}_e}{\|\boldsymbol{Q}_e\|} & \text{if } \|\boldsymbol{H}^t\| = 0, \\ \frac{\boldsymbol{H}^t}{\|\boldsymbol{H}^t\|} & \text{if } \|\boldsymbol{H}^t\| \neq 0. \end{cases} \tag{93}$$

We note that according to the above discussion, the tensor $\boldsymbol{N}$ and consequently the tensor $\boldsymbol{X}$ are well-defined, non-singular and continuous.

We finally summarize the proposed finite strain constitutive model for shape memory alloys in Table 3. We recall that, for simplicity, all inelastic quantities are denoted without a bar symbol.

5.3. Solution algorithm

As usual in computational inelasticity problems, to solve the time-discrete constitutive model we use an elastic predictor-inelastic corrector procedure. The algorithm consists of evaluating an elastic trial state, in which the internal variable remains constant, and of verifying the admissibility of the trial function. If the trial state is admissible, the step is elastic; otherwise, the step is inelastic and the transformation internal variable has to be updated through integration of the evolution equation.

We now substitute (84) into (78) and obtain the time-discrete tensorial evolution equation as

$$-\log\left(\overline{\boldsymbol{U}}^t\overline{\boldsymbol{C}}_n^{t^{-1}}\overline{\boldsymbol{U}}^t\right) + 2\Delta\lambda\frac{\boldsymbol{Z}}{\|\boldsymbol{Z}\|} = \boldsymbol{0}. \tag{94}$$

In order to solve the inelastic step, we use another predictor–corrector scheme, that is, we assume $\gamma = 0$ (i.e., we predict an unsaturated transformation strain case with $\|\boldsymbol{H}^t\| \leqslant \varepsilon_L$) and we solve the following system of nonlinear equations (we refer to this system as *PT1* system):

$$\begin{cases} \boldsymbol{R}^t = -\log\left(\boldsymbol{U}^t\boldsymbol{C}_n^{t^{-1}}\boldsymbol{U}^t\right) + 2\Delta\lambda\boldsymbol{W} = \boldsymbol{0}, \\ R^\zeta = \|\boldsymbol{Z}\| - R = 0, \end{cases} \tag{95}$$

where $\boldsymbol{W} = \boldsymbol{Z}/\|\boldsymbol{Z}\|$. If the solution is not admissible (i.e., $\|\boldsymbol{H}^t\|_{PT1} > \varepsilon_L$), we assume $\gamma > 0$ (i.e., we consider a saturated transformation case with $\|\boldsymbol{H}^t\| = \varepsilon_L$) and we solve the following system of nonlinear equations (we refer to this system as *PT2* system):

[15] To avoid confusing, we remark that we have used superscript "t" in place of "in" in this section.

Table 3
Finite-strain SMA constitutive model in the time-continuous frame.

External variables: $\overline{\boldsymbol{C}},\ J,\ T$
Internal variable: $\boldsymbol{U}^t$
Stress quantities: $\boldsymbol{Q} = \mu \log(\boldsymbol{U}^{t^{-1}}\overline{\boldsymbol{C}}\boldsymbol{U}^{t^{-1}}) = 2\mu\mathscr{H}^e$
$\boldsymbol{X} = h_k\boldsymbol{H}^t + (\tau_M(T) + \gamma)\boldsymbol{N}$
$\boldsymbol{Z} = \boldsymbol{Q} - \boldsymbol{X}$
$\boldsymbol{S} = J^{-2/3}\overline{\boldsymbol{C}}^{-1}(K\log(J)\boldsymbol{1} + \boldsymbol{U}^t\boldsymbol{Q}\boldsymbol{U}^{t^{-1}})$
with
$\boldsymbol{H}^t = \log(\boldsymbol{U}^{in}),\quad \mathscr{H}^e = \frac{1}{2}\log(\boldsymbol{U}^{t^{-1}}\overline{\boldsymbol{C}}\boldsymbol{U}^{t^{-1}})$
$\boldsymbol{N} = \begin{cases} \frac{\boldsymbol{Q}_e}{\|\boldsymbol{Q}_e\|} & \text{if } \|\boldsymbol{H}^t\| = 0 \\ \frac{\boldsymbol{H}^t}{\|\boldsymbol{H}^t\|} & \text{if } \|\boldsymbol{H}^t\| \neq 0 \end{cases}$
$\boldsymbol{Q}^e = 2\mu\overline{\boldsymbol{H}}$
Evolution equation: $\dot{\boldsymbol{C}}^t = 2\dot{\lambda}\boldsymbol{U}^t\frac{\boldsymbol{Z}}{\|\boldsymbol{Z}\|}\boldsymbol{U}^t$
Limit function: $F = \|\boldsymbol{Z}\| - R$
Kuhn–Tucker conditions: $F \leqslant 0,\ \dot{\lambda} \geqslant 0,\ \dot{\lambda}F = 0$

$$\begin{cases} \boldsymbol{R}^t = -\log\left(\boldsymbol{U}^t\boldsymbol{C}_n^{t^{-1}}\boldsymbol{U}^t\right) + 2\Delta\lambda\boldsymbol{W} = \boldsymbol{0}, \\ R^\zeta = \|\boldsymbol{Z}\| - R = 0, \\ R^\gamma = \|\boldsymbol{H}^t\| - \varepsilon_L = 0. \end{cases} \tag{96}$$

Solution of Eqs. (95) and (96) is in general approached through a straightforward Newton–Raphson method and it is not characterized by special difficulties except for the cases in which the transformation strain vanishes. Accordingly, in the following, we specifically focus on the nucleation ($\boldsymbol{H}_n^t = \boldsymbol{0}$) and completion ($\boldsymbol{H}^t = \boldsymbol{0}$) cases and construct the solution algorithm. We refer to Arghavani et al. (2010b) for more details on the numerical implementation.

5.4. Considerations on nucleation-completion condition

We first investigate the trial value of the limit function in the nucleation case as

$$f^{TR} = |\|\boldsymbol{Q}_e\| - \tau_M(T)| - R = \|\boldsymbol{Q}_e\| - \tau_M(T) - R > 0, \tag{97}$$

where a subscript *TR* indicates a trial value. We may thus introduce the following *nucleation condition*:

$$\|\boldsymbol{Q}_e\| > \tau_M(T) + R \quad \text{and} \quad \|\boldsymbol{H}_n^t\| = 0. \tag{98}$$

In the solution procedure, when $\|\boldsymbol{H}_n^t\| = 0$ we check the nucleation condition and if not satisfied, we assume an elastic behavior.

We remark that, to avoid singularity in system (95) for the nucleation case, it is necessary to use a nonzero initial (guess) transformation strain. Since, we know the initial transformation strain direction from (93), the only unknown for constructing an initial guess is its norm; if we denote with $\bar{q}$ its value, we can use the following initial guess for the nucleation case:

$$\boldsymbol{H}_0^t = \log(\boldsymbol{U}_0^t) \simeq \boldsymbol{U}_0^t - \boldsymbol{1} = \bar{q}\boldsymbol{N} \Rightarrow \boldsymbol{U}_0^t = \boldsymbol{1} + \bar{q}\boldsymbol{N}, \tag{99}$$

where a subscript 0 denotes the initial guess. A value of 10^{-4} could be an appropriate choice for $\bar{q}$.

We now focus on the completion case, i.e., $\boldsymbol{H}_n^t \neq \boldsymbol{0}$ but $\boldsymbol{H}^t = \boldsymbol{0}$. To this end, we consider Eqs. (76) or (77) and substitute $\boldsymbol{U}^t = \boldsymbol{1}$ (as it happens for the completion case) to obtain:

$$\Delta\zeta\boldsymbol{A} = \log\left(\boldsymbol{C}_n^{t^{-1}}\right) = -2\boldsymbol{H}_n^t, \quad \boldsymbol{A} = 2\frac{\boldsymbol{Z}}{\|\boldsymbol{Z}\|}, \quad \boldsymbol{Z} = \boldsymbol{Q}_e - \tau_M\boldsymbol{N}. \tag{100}$$

To this end, using $(100)_{1,2}$ which define the $\boldsymbol{Z}$ direction and considering the limit function (84), we conclude:

$$\boldsymbol{Z} = -R\frac{\boldsymbol{H}_n^t}{\|\boldsymbol{H}_n^t\|} = -R\boldsymbol{N}^{TR}, \tag{101}$$

substituting (101) in $(100)_3$, we obtain:

$$\boldsymbol{Q}_e + R\boldsymbol{N}^{TR} = \tau_M\boldsymbol{N}. \tag{102}$$

Finally taking the norm of both sides of Eq. (102), we define the following *completion condition*:

$$\|\boldsymbol{Q}_e + R\boldsymbol{N}^{TR}\| \leqslant \tau_M, \quad \|\boldsymbol{H}_n^t\| \neq 0. \tag{103}$$

Therefore, in the solution procedure we also should check the completion condition and, if it is satisfied, we simply update the internal variable by setting $\boldsymbol{U}^t = \boldsymbol{1}$.

Table 4 finally presents the branch detection and the solution algorithm. For more details and discussions on the algorithm robustness, we refer to Arghavani et al. (2010b).

5.5. Consistent tangent matrix

In the following, we linearize the nonlinear equations as it is required for the iterative Newton–Raphson method. For brevity, we report the construction of the tangent matrix only for the case of the saturated phase transformation, corresponding to (96). Linearizing (96), we obtain:

$$\begin{cases} \boldsymbol{R}^t + \boldsymbol{R}^t_{,\boldsymbol{U}^t} : d\boldsymbol{U}^t + \boldsymbol{R}^t_{,\Delta\lambda} d\Delta\lambda + \boldsymbol{R}^t_{,\gamma} d\gamma = \boldsymbol{0}, \\ R^\lambda + R^\lambda_{,\boldsymbol{U}^t} : d\boldsymbol{U}^t + R^\lambda_{,\Delta\lambda} d\Delta\lambda + R^\lambda_{,\gamma} d\gamma = 0, \\ R^\gamma + R^\gamma_{,\boldsymbol{U}^t} : d\boldsymbol{U}^t + R^\gamma_{,\Delta\lambda} d\Delta\lambda + R^\gamma_{,\gamma} d\gamma = 0, \end{cases} \tag{104}$$

where subscripts following a comma indicate differentiation with respect to that quantity. The derivatives appearing in the above equation are detailed in Arghavani (2010).

Utilizing the linearized form (104), after converting it to a matrix form, a system of eight nonlinear scalar equations is solved to obtain $d\boldsymbol{U}^t$, $d\Delta\lambda$ and $d\gamma$.

We now address the construction of the tangent tensor consistent with the time-discrete constitutive model. The use of a consistent tensor preserves the quadratic convergence of the Newton–Raphson method for the incremental solution of the global time-discrete problem, as in the framework of a finite element scheme.

The consistent tangent is computed by linearizing the second Piola-Kirchhof tensor, i.e.

$$d\boldsymbol{S} = \mathbb{D} : d\boldsymbol{E} = \frac{1}{2}\mathbb{D} : d\boldsymbol{C}. \tag{105}$$

Recalling that $\boldsymbol{S}$ is a function of J, $\overline{\boldsymbol{C}}$ and $\boldsymbol{U}^t$, we can write:

$$d\boldsymbol{S} = \frac{\partial \boldsymbol{S}}{\partial J} dJ + \frac{\partial \boldsymbol{S}}{\partial \overline{\boldsymbol{C}}} : d\overline{\boldsymbol{C}} + \frac{\partial \boldsymbol{S}}{\partial \boldsymbol{U}^t} : d\boldsymbol{U}^t. \tag{106}$$

The following relations express dJ and $d\overline{\boldsymbol{C}}$ in terms of $d\boldsymbol{C}$ (Holzapfel, 2000):

$$dJ = \frac{J^{1/3}}{2}\overline{\boldsymbol{C}}^{-1} : d\boldsymbol{C} \quad \text{and} \quad d\overline{\boldsymbol{C}} = J^{-2/3}\mathbb{P} : d\boldsymbol{C}, \tag{107}$$

where,

$$\mathbb{P} = \mathbb{I} - \frac{1}{3}\overline{\boldsymbol{C}} \otimes \overline{\boldsymbol{C}}^{-1}, \tag{108}$$

and $\mathbb{I}$ denotes the fourth-order identity tensor.

Table 4
Branch detection procedure and solution algorithm.

1. Compute $\boldsymbol{C} = \boldsymbol{F}^T\boldsymbol{F}$ then $J = \sqrt{\det \boldsymbol{C}}$ and $\overline{\boldsymbol{C}} = J^{-2/3}\boldsymbol{C}$
2. Compute $\boldsymbol{Q}_e$
3. **if** ($\|\boldsymbol{Q}_e\| < \tau_M + R$ and $\|\boldsymbol{H}^t_n\| = 0$) **then**
   set $\boldsymbol{U}^t = \boldsymbol{1}$
   else
   use (93) and set $\boldsymbol{U}^{tTR} = \boldsymbol{U}^t_n$ to compute f^{TR} and trial solution
   if ($f^{TR} < 0$) **then**
   set trial solution as the problem solution, i.e., $\boldsymbol{U}^t = \boldsymbol{U}^{tTR}$
   else if (completion condition (103)) **then**
   set $\boldsymbol{U}^t = \boldsymbol{1}$
   else
   set $\boldsymbol{U}^t_0 = \boldsymbol{U}^t_n$ and $\Delta\lambda_0 = 0$.
   if $\|\boldsymbol{H}^t_n\| = 0$ **then** set $\boldsymbol{U}^t_0$ value by (99)
   solve PT1
   if ($\|\boldsymbol{H}^t\|_{PT1} < \varepsilon_L$) **then**
   set PT1 solution as the solution: i.e., $\boldsymbol{U}^t = \boldsymbol{U}^t_{PT1}$
   else
   set $\boldsymbol{U}^t_0 = \boldsymbol{U}^t_{PT1}$, $\Delta\lambda_0 = \Delta\lambda_{PT1}$ and $\gamma_0 = 0$, then solve PT2
   set $\boldsymbol{U}^t = \boldsymbol{U}^t_{PT2}$
   end if
   end if
   end if
   end if

We now consider Eq. (96) as a function of $\overline{\boldsymbol{C}}$, $\boldsymbol{U}^t$, $\Delta\lambda$ and γ, and then the corresponding linearization gives:

$$\begin{cases} \boldsymbol{R}^t_{,\overline{\boldsymbol{C}}} : d\overline{\boldsymbol{C}} + \boldsymbol{R}^t_{,\boldsymbol{U}^t} : d\boldsymbol{U}^t + \boldsymbol{R}^t_{,\Delta\lambda}\, d\Delta\lambda + \boldsymbol{R}^t_{,\gamma}\, d\gamma = \boldsymbol{0}, \\ R^\lambda_{,\overline{\boldsymbol{C}}} : d\overline{\boldsymbol{C}} + R^\lambda_{,\boldsymbol{U}^t} : d\boldsymbol{U}^t + R^\lambda_{,\Delta\lambda}\, d\Delta\lambda + R^\lambda_{,\gamma}\, d\gamma = 0, \\ R^\gamma_{,\overline{\boldsymbol{C}}} : d\overline{\boldsymbol{C}} + R^\gamma_{,\boldsymbol{U}^t} : d\boldsymbol{U}^t + R^\gamma_{,\Delta\lambda}\, d\Delta\lambda + R^\gamma_{,\gamma}\, d\gamma = 0. \end{cases} \tag{109}$$

Recasting (109) into a matrix form, we obtain:

$$\begin{bmatrix} d\boldsymbol{U}^t \\ d\lambda \\ d\gamma \end{bmatrix} = -\begin{bmatrix} \boldsymbol{R}^t_{,\boldsymbol{U}^t} & \boldsymbol{R}^t_{,\Delta\lambda} & \boldsymbol{R}^t_{,\gamma} \\ R^\lambda_{,\boldsymbol{U}^t} & R^\lambda_{,\Delta\lambda} & R^\lambda_{,\gamma} \\ R^\gamma_{,\boldsymbol{U}^t} & R^\gamma_{,\Delta\lambda} & R^\gamma_{,\gamma} \end{bmatrix}^{-1} \begin{bmatrix} \boldsymbol{R}^t_{,\overline{\boldsymbol{C}}} \\ R^\lambda_{,\overline{\boldsymbol{C}}} \\ R^\gamma_{,\overline{\boldsymbol{C}}} \end{bmatrix} [d\overline{\boldsymbol{C}}], \tag{110}$$

where we have used $[\cdot]$ to denote the matrix form of the tensorial argument. Now, using (110), we can compute the matrix $[\mathbb{B}]$ (the matrix form of the fourth-order tensor $\mathbb{B}$) such that:

$$[d\boldsymbol{U}^t] = [\mathbb{B}][d\overline{\boldsymbol{C}}] \quad \text{or} \quad d\boldsymbol{U}^t = \mathbb{B} : d\overline{\boldsymbol{C}}. \tag{111}$$

We then substitute (107) and $(111)_2$ into (105) to obtain the consistent tangent as

$$\mathbb{D} = J^{1/3}\boldsymbol{J} \otimes \overline{\boldsymbol{C}}^{-1} + 2J^{-2/3}(\mathbb{S} + \mathbb{T} : \mathbb{B}) : \mathbb{P}, \tag{112}$$

where the second-order tensor $\partial\boldsymbol{S}/\partial J$ as well as the fourth-order tensors $\partial\boldsymbol{S}/\partial\overline{\boldsymbol{C}}$ and $\partial\boldsymbol{S}/\partial\boldsymbol{U}^t$ are denoted by $\boldsymbol{J}$, $\mathbb{S}$ and $\mathbb{T}$, respectively.

6. Numerical examples

In this section, we solve some boundary value problems to show the proposed model capabilities as well as the proposed integration algorithm and the solution procedure. A uni-axial test on a cube, crimping of a pseudo-elastic medical stent and a helical spring actuator are simulated to show the model capability of capturing both pseudo-elasticity and shape memory effect.

For all simulations, we use the commercial nonlinear finite element software ABAQUS/Standard, implementing the described algorithm within a user-defined subroutine UMAT.

The following material properties, typical of NiTi,[16] are adopted in all the simulations of this paper:

$$E = 51700\ \text{MPa}, \quad \nu = 0.3, \quad h_k = 1000\ \text{MPa}, \quad \varepsilon_L = 10\%,$$
$$\beta = 5.6\ \text{MPa}\,^\circ\text{C}^{-1}, \quad T_0 = -25\,^\circ\text{C}, \quad R = 140\ \text{MPa}, \quad A_f = 0\,^\circ\text{C}, \quad M_f = -25\,^\circ\text{C}.$$

where E and ν are the elastic modulus and the Poisson ratio, respectively.

6.1. Uni-axial test

We simulate a single element unit cube under an applied force on one face while the opposite face is fixed. The applied force is increased from zero to a maximum value of 1500 N and subsequently decreased to zero and increased in the opposite direction to a value of 1500 N and finally decreased back to zero. Fig. 1(a) and (b) show the SMA behavior at 37 and -25 °C, respectively. We observe the pseudo-elastic behavior in Fig. 1(a) where the temperature is above the austenite finish temperature while in Fig. 1(b) the material does not recover the original shape after unloading; however it can be recovered by heating above the austenite finish temperature (shape memory effect).

6.2. Pseudo-elastic stent

In this example, the crimping of a pseudo-elastic medical stent is simulated at a temperature of 37 °C. To this end a medical stent with 0.216 mm thickness and an initial outer diameter of 6.3 mm (Fig. 2(a)) is crimped to an outer diameter of 1.5 mm. Utilizing the ABAQUS/Standard contact module, the contact between the catheter (with initial diameter of 6.5 mm) and the stent is considered in the simulation. A radial displacement of 2.5 mm is applied to the catheter and is then released to reach the initial diameter. In this process, the stent recovers its original shape after unloading. Fig. 2(b) shows the stent deformed shape when fully crimped. Moreover, Fig. 3 reports the von-Mises stress at the critical point A (shown in Fig. 2(b)) versus the reduction percentage in catheter diameter.

[16] See, e.g., www.shape-memory-alloys.com

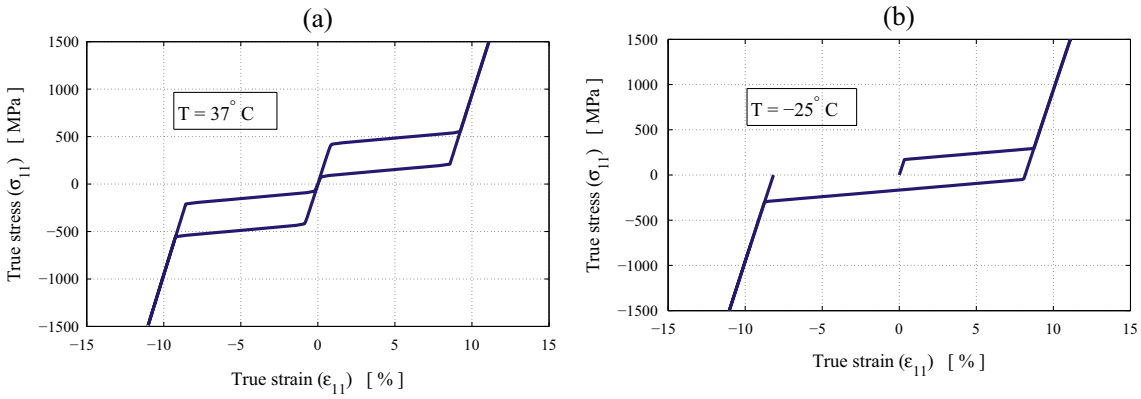

Fig. 1. Illustration of the material behavior under uni-axial force-controlled test: (a) pseudo-elasticity at $T = 37\ ^{\circ}C$, (b) shape memory effect at $T = -25\ ^{\circ}C$.

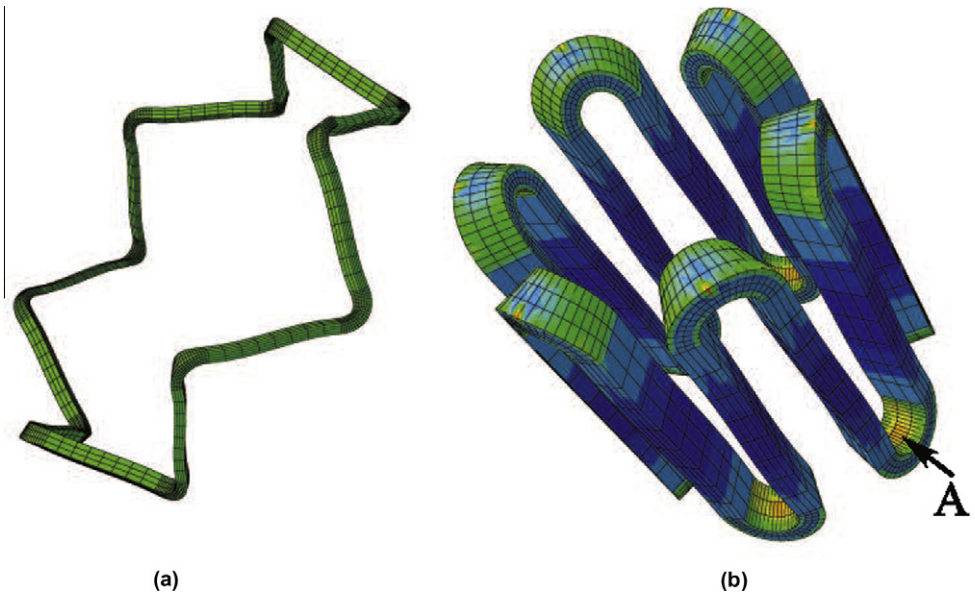

Fig. 2. Pseudo-elastic stent crimping: (a) initial geometry, (b) crimped shape.

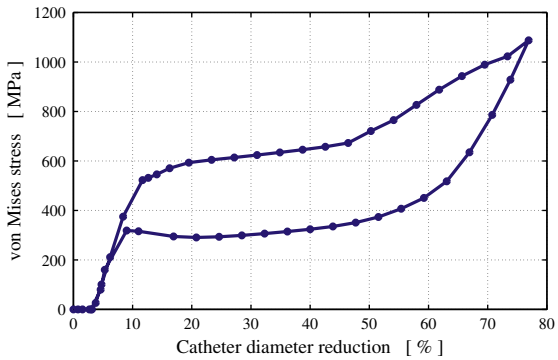

Fig. 3. von-Mises stress versus percentage of catheter diameter reduction (at point *A* shown in Fig. 2(b)).

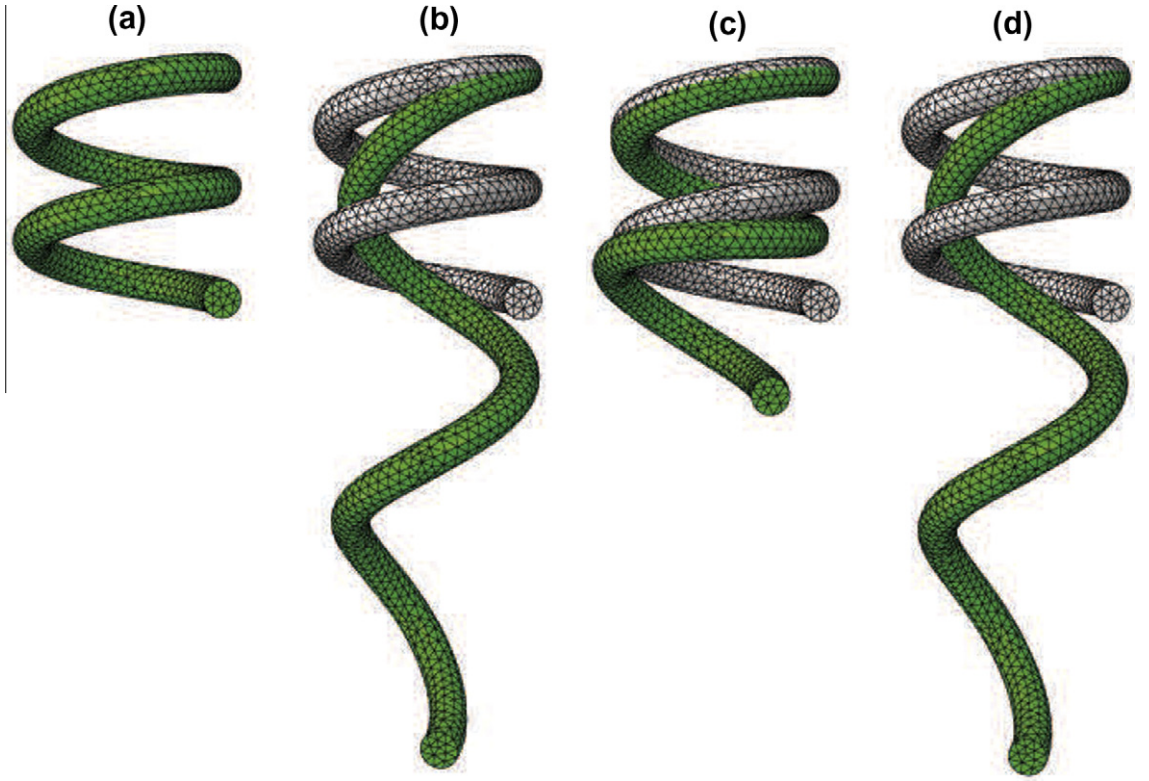

Fig. 4. Spring actuator: (A) initial geometry and mesh, (B) deformed shape due to the weight application at $T = -25$ °C, (C) spring shape recovery and weight lifting due to heating to $T = 75$ °C, (D) spring stretching due to cooling to $T = -25$ °C.

6.3. Spring actuator

In order to investigate the shape memory effect, a vertical helical spring (with a wire diameter of 4 mm, a spring external diameter of 24 mm, a pitch size of 12 mm and with two coils and an initial length of 28 mm) is simulated using 9453 quadratic tetrahedron (C3D10) elements and 15764 nodes (Fig. 4A). The spring is loaded by a weight $W = 244$ N in martensite state at $T = -25$ °C (Fig. 4B), If the stress applied by the weight is less than the alloy recovery stress, heating the material above A_f induces the inverse phase transformation and the spring lifts the weight (Fig. 4C). Moreover, cooling below M_f the transformation from austenite to martensite takes place and the weight stretches again the spring (Fig. 4D); accordingly, a repeatable two-way motion takes place.

We remark that in the analysis, we assume that during each time step the temperature is uniform in the material body, i.e., we neglect the thermo-mechanical coupling.

Fig. 5a shows the loading history during the simulation. In Fig. 5(b), we plot the vertical displacement versus temperature. It is observed that applying a temperature cycle between −25 and 75 °C, the spring actuator traverse a length of 37 mm.

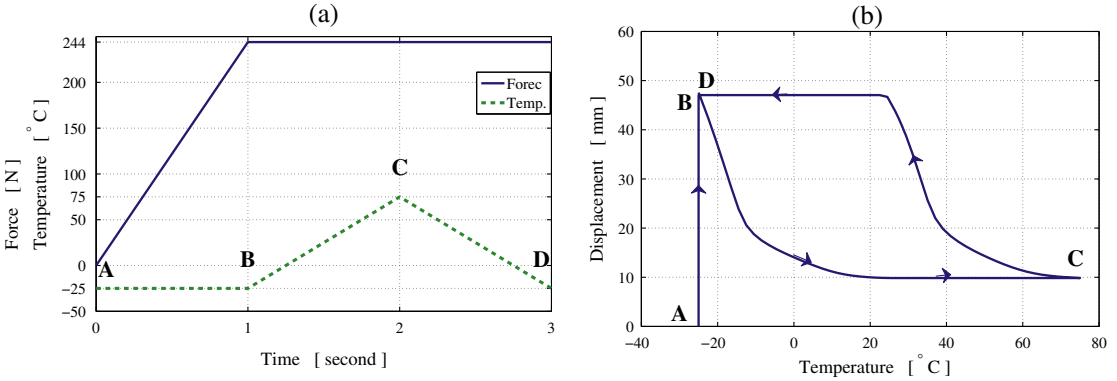

Fig. 5. (a) Loading history during simulation, (b) vertical displacement of the lower loaded end of spring versus temperature variation.

7. Summary

In this work, we propose a finite strain Hencky-based kinematic-hardening constitutive model. The derivation is based on the multiplicative decomposition of the deformation gradient into elastic and inelastic parts. Moreover, in the derivations, we use the isotropic property and the fact that the corotational rate of the Eulerian logarithmic strain associated with the so-called logarithmic spin is the strain rate tensor. The developed constitutive model has a Lagrangian form. Moreover, defining an elastic-like strain tensor, the developed finite strain constitutive model takes a structure similar to that of small strain model has, thanks to Hencky strain. Introducing a logarithmic mapping, we also present the time-discrete constitutive model. We then apply the developed model to shape memory alloys (SMAs) and present a well-defined, non-singular constitutive model. We finally discuss solution algorithm and consistent matrix derivation and simulate several SMA boundary value problems, demonstrating the modeling as well as numerical implementation capabilities.

Acknowledgements

J. Arghavani has been partially supported by Iranian Ministry of Science, Research and Technology, and partially by Dipartimento di Meccanica Strutturale, Università degli Studi di Pavia.

F. Auricchio has been partially supported by the Cariplo Foundation through the project number: 2009.2822; by the Ministero dell'Istruzione, dell'Università e della Ricerca through the project number: 2008MRKXLX; and by the European Research Council through the Starting Independent Research Grant "BioSMA: Mathematics for Shape Memory Technologies in Biomechanics".

Appendix A

In this appendix, we present details of the relations we used in the previous sections. The logarithm of a tensor $\mathcal{B}$ can be expanded as follows:

$$\log \mathcal{B} = (\mathcal{B}-\mathbf{1}) - \frac{1}{2}(\mathcal{B}-\mathbf{1})^2 + \frac{1}{3}(\mathcal{B}-\mathbf{1})^3 - \frac{1}{4}(\mathcal{B}-\mathbf{1})^4 + \cdots, \tag{113}$$

which is absolutely convergent if $\|\mathcal{B}-\mathbf{1}\| \leqslant 1$, but $\mathcal{B} \neq \mathbf{0}$.[17]

We substitute $\bar{\boldsymbol{b}}^e$ for $\mathcal{B}$ in (113) to obtain:

$$\log \bar{\boldsymbol{b}}^e = 2\bar{\boldsymbol{h}}^e = (\bar{\boldsymbol{b}}^e-\mathbf{1}) - \frac{1}{2}(\bar{\boldsymbol{b}}^e-\mathbf{1})^2 + \frac{1}{3}(\bar{\boldsymbol{b}}^e-\mathbf{1})^3 - \frac{1}{4}(\bar{\boldsymbol{b}}^e-\mathbf{1})^4 + \cdots. \tag{114}$$

We now show that $\overline{\boldsymbol{F}}^{e^T}\boldsymbol{s}\overline{\boldsymbol{F}}^{e^{-T}}$ is a symmetric tensor. To this end we substitute (40) into $(30)_2$ to obtain:

$$\boldsymbol{s} = \frac{\partial \psi^e}{\partial \bar{\boldsymbol{h}}^e} = \alpha_1\mathbf{1} + 2\alpha_2\bar{\boldsymbol{h}}^e + 4\alpha_3\bar{\boldsymbol{h}}^{e^2}. \tag{115}$$

We then observe that:

$$\overline{\boldsymbol{F}}^{e^T}(\bar{\boldsymbol{b}}^e-\mathbf{1})^n\overline{\boldsymbol{F}}^{e^{-T}} = (\overline{\boldsymbol{C}}^e-\mathbf{1})^n, \tag{116}$$

where n is a positive integer number. Substituting (116) into (114), we conclude:

$$\overline{\boldsymbol{F}}^{e^T}\bar{\boldsymbol{h}}^e\overline{\boldsymbol{F}}^{e^{-T}} = \overline{\boldsymbol{H}}^e \quad \text{and} \quad \overline{\boldsymbol{F}}^{e^T}\bar{\boldsymbol{h}}^{e^2}\overline{\boldsymbol{F}}^{e^{-T}} = \overline{\boldsymbol{H}}^{e^2}. \tag{117}$$

We now combine (117) and (115) to obtain:

$$\overline{\boldsymbol{F}}^{e^T}\boldsymbol{s}\overline{\boldsymbol{F}}^{e^{-T}} = \alpha_1\mathbf{1} + 2\alpha_2\overline{\boldsymbol{H}}^e + 4\alpha_3\overline{\boldsymbol{H}}^{e^2}. \tag{118}$$

According to (118), we conclude that $\overline{\boldsymbol{F}}^{e^T}\boldsymbol{s}\overline{\boldsymbol{F}}^{e^{-T}}$ is a symmetric tensor.

We now show that $\bar{\boldsymbol{h}}^e = \frac{1}{2}\overline{\boldsymbol{F}}^{-T}\log(\overline{\boldsymbol{C}}\overline{\boldsymbol{C}}^{in^{-1}})\overline{\boldsymbol{F}}^T$. To this end, we observe that:

$$\bar{\boldsymbol{b}}^e = \overline{\boldsymbol{F}}\overline{\boldsymbol{C}}^{in^{-1}}\overline{\boldsymbol{F}}^T = \overline{\boldsymbol{F}}^{-T}\overline{\boldsymbol{C}}\overline{\boldsymbol{C}}^{in^{-1}}\overline{\boldsymbol{F}}^T. \tag{119}$$

According to (119), we conclude:

$$(\bar{\boldsymbol{b}}^e-\mathbf{1})^n = \overline{\boldsymbol{F}}^{-T}\left(\overline{\boldsymbol{C}}\overline{\boldsymbol{C}}^{in^{-1}}-\mathbf{1}\right)^n\overline{\boldsymbol{F}}^T. \tag{120}$$

We now substitute (120) into (114) and obtain:

$$\bar{\boldsymbol{h}}^e = \frac{1}{2}\overline{\boldsymbol{F}}^{-T}\log(\overline{\boldsymbol{C}}\overline{\boldsymbol{C}}^{in^{-1}})\overline{\boldsymbol{F}}^T. \tag{121}$$

[17] Similar expansion can be considered if $\|\mathcal{B}-\mathbf{1}\| > 1$, for example if $\|\mathcal{B}-2\mathbf{1}\| \leqslant 1$, we use: $\log\mathcal{B} = \log(2)\mathbf{1} + (\mathcal{B}-2\mathbf{1}) - \frac{1}{2}(\mathcal{B}-2\mathbf{1})^2 + \frac{1}{3}(\mathcal{B}-2\mathbf{1})^3 - \frac{1}{4}(\mathcal{B}-2\mathbf{1})^4 + \cdots$.

Substituting (121) into (117) we also obtain:

$$\overline{\boldsymbol{F}}^{in^T}\overline{\boldsymbol{H}}^{e}\overline{\boldsymbol{F}}^{in}=\frac{1}{2}\log\left(\overline{\boldsymbol{C}}\overline{\boldsymbol{C}}^{in^{-1}}\right)\overline{\boldsymbol{C}}^{in}. \tag{122}$$

We now mention the following properties:

$$\begin{aligned}&\overline{\boldsymbol{C}}\overline{\boldsymbol{C}}^{in^{-1}}-\mathbf{1}=\overline{\boldsymbol{U}}^{in}\left(\overline{\boldsymbol{U}}^{in^{-1}}\overline{\boldsymbol{C}}\overline{\boldsymbol{U}}^{in^{-1}}-\mathbf{1}\right)\overline{\boldsymbol{U}}^{in^{-1}},\\&\left(\overline{\boldsymbol{C}}\overline{\boldsymbol{C}}^{in^{-1}}-\mathbf{1}\right)^{n}=\overline{\boldsymbol{U}}^{in}\left(\overline{\boldsymbol{U}}^{in^{-1}}\overline{\boldsymbol{C}}\overline{\boldsymbol{U}}^{in^{-1}}-\mathbf{1}\right)^{n}\overline{\boldsymbol{U}}^{in^{-1}},\end{aligned} \tag{123}$$

Finally, substitution of (123) into logarithmic expansion (113) yields:

$$\log(\overline{\boldsymbol{C}}\overline{\boldsymbol{C}}^{in^{-1}})=\overline{\boldsymbol{U}}^{in}\log\left(\overline{\boldsymbol{U}}^{in^{-1}}\overline{\boldsymbol{C}}\overline{\boldsymbol{U}}^{in^{-1}}\right)\overline{\boldsymbol{U}}^{in^{-1}}. \tag{124}$$

We assumed $G(\boldsymbol{\alpha},q)$ to be an isotropic function of its argument, therefore, considering representation theorem, we may write:

$$\frac{\partial G(\boldsymbol{\alpha},q)}{\partial\boldsymbol{\alpha}}=c_1\mathbf{1}+c_2\boldsymbol{\alpha}+c_3\boldsymbol{\alpha}^2, \tag{125}$$

where the coefficients c_1, c_2 and c_3 are functions of the invariants of $\boldsymbol{\alpha}$ and q. We now multiply (125) from left and right by $\overline{\boldsymbol{F}}^{in^T}$ and $\overline{\boldsymbol{F}}^{in}$, respectively:

$$\overline{\boldsymbol{F}}^{in^T}\frac{\partial G(\boldsymbol{\alpha},q)}{\partial\boldsymbol{\alpha}}\overline{\boldsymbol{F}}^{in}=c_1\overline{\boldsymbol{F}}^{in^T}\overline{\boldsymbol{F}}^{in}+c_2\overline{\boldsymbol{F}}^{in^T}\boldsymbol{\alpha}\overline{\boldsymbol{F}}^{in}+c_3\overline{\boldsymbol{F}}^{in^T}\boldsymbol{\alpha}^2\overline{\boldsymbol{F}}^{in}. \tag{126}$$

We now use (60) in (126) to obtain:

$$\overline{\boldsymbol{F}}^{in^T}\frac{\partial G(\boldsymbol{\alpha},q)}{\partial\boldsymbol{\alpha}}\overline{\boldsymbol{F}}^{in}=c_1\overline{\boldsymbol{U}}^{in^2}+c_2\overline{\boldsymbol{U}}^{in}\boldsymbol{Z}\overline{\boldsymbol{U}}^{in}+c_3\overline{\boldsymbol{U}}^{in}\boldsymbol{Z}^2\overline{\boldsymbol{U}}^{in}=\overline{\boldsymbol{U}}^{in}\left(c_1\mathbf{1}+c_2\boldsymbol{Z}+c_3\boldsymbol{Z}^2\right)\overline{\boldsymbol{U}}^{in}. \tag{127}$$

In Eq. (60) we showed that the invariants of $\boldsymbol{\alpha}$ are equal to those of $\boldsymbol{Z}$. Thus, we conclude that the terms inside the parenthesis in (127) represent $\frac{\partial G(\boldsymbol{Z},q)}{\partial\boldsymbol{Z}}$. Therefore, we can write:

$$\overline{\boldsymbol{F}}^{in^T}\frac{\partial G(\boldsymbol{\alpha},q)}{\partial\boldsymbol{\alpha}}\overline{\boldsymbol{F}}^{in}=\overline{\boldsymbol{U}}^{in}\frac{\partial G(\boldsymbol{Z},q)}{\partial\boldsymbol{Z}}\overline{\boldsymbol{U}}^{in}. \tag{128}$$

References

Anand, L., 1979. On h. henckys approximate strain-energy function for moderate deformations. ASME Journal of Applied Mechanics 46, 78–82.

Anand, L., 1986. Moderate deformations in extension–torsion of incompressible isotropic elastic materials. Mechanics and Physics of Solids 34, 293–304.

Arghavani, J., 2010. Thermo-mechanical behavior of shape memory alloys under multiaxial loadings: constitutive modeling and numerical inplementation at small and finite strains. PhD Thesis. Sharif University of Technology, Iran.

Arghavani, J., Auricchio, F., Naghdabadi, R., Reali, A., 2010a. An improved, fully symmetric, finite strain phenomenological constitutive model for shape memory alloys. Finite Elements in Analysis and Design. doi:10.1016/j.finel.2010.09.001.

Arghavani, J., Auricchio, F., Naghdabadi, R., Reali, A., 2010b. On the robustness and efficiency of integration algorithms for a 3D finite strain phenomenological SMA constitutive model. International Journal for Numerical Methods in Engineering. doi:10.1002/nme.2964.

Arghavani, J., Auricchio, F., Naghdabadi, R., Reali, A., Sohrabpour, S., 2010c. A 3D phenomenological constitutive model for shape memory alloys under multiaxial loadings. International Journal of Plasticity 26, 976–991.

Arghavani, J., Auricchio, F., Naghdabadi, R., Reali, A., Sohrabpour, S., 2010d. A 3D finite strain phenomenological constitutive model for shape memory alloys considering martensite reorientation. Continuum Mechanics and Thermodynamics 22, 345–362.

Auricchio, F., 2001. A robust integration-algorithm for a finite-strain shape-memory-alloy superelastic model. International Journal of Plasticity 17, 971–990.

Auricchio, F., Marfia, S., Sacco, E., 2003. Modelling of SMA materials: training and two way memory effects. Computers and Structures 81, 2301–2317.

Auricchio, F., Petrini, L., 2002. Improvements and algorithmical considerations on a recent three-dimensional model describing stress-induced solid phase transformations. International Journal for Numerical Methods in Engineering 55, 1255–1284.

Auricchio, F., Petrini, L., 2004a. A three-dimensional model describing stress-temperature induced solid phase transformations: thermomechanical coupling and hybrid composite applications. International Journal for Numerical Methods in Engineering 61, 716–737.

Auricchio, F., Petrini, L., 2004b. A three-dimensional model describing stress-temperature induced solid phase transformations: solution algorithm and boundary value problems. International Journal for Numerical Methods in Engineering 61, 807–836.

Auricchio, F., Reali, A., Stefanelli, U., 2007. A three-dimensional model describing stress-induced solid phase transformation with permanent inelasticity. International Journal of Plasticity 23, 207–226.

Auricchio, F., Taylor, R.L., 1997. Shape-memory alloys: modelling and numerical simulations of the finite-strain superelastic behavior. Computer Methods in Applied Mechanics and Engineering 143, 175–194.

Bekker, A., Brinson, L.C., 1997. Temperature-induced phase transformation in a shape memory alloy: phase diagram based kinetics approach. Journal of the Mechanics and Physics of Solids 45, 949–988.

Bouvet, C., Calloch, S., Lexcellent, C., 2002. Mechanical behavior of a Cu–Al–Be shape memory alloy under multiaxial proportional and nonproportional loadings. Journal of Engineering Materials and Technology 124, 112–124.

Bouvet, C., Calloch, S., Lexcellent, C., 2004. A phenomenological model for pseudoelasticity of shape memory alloys under multiaxial proportional and nonproportional loadings. European Journal of Mechanics A – Solids 23, 37–61.

Bruhns, O.T., Xiao, H., Meyers, A., 1999. Self-consistent eulerian rate type elasto-plasticity models based upon the logarithmic stress rate. International Journal of Plasticity 15, 479–520.

Christ, D., Reese, S., 2009. A finite element model for shape memory alloys considering thermomechanical couplings at large strains. International Journal of Solids and Structures 46, 3694–3709.

Criscione, J.C., Humphrey, J.D., Douglas, A.S., Hunter, W.C., 2000. An invariant basis for natural strain which yields orthogonal stress response terms in isotropic hyperelasticity. Journal of the Mechanics and Physics of Solids 48, 2445–2465.
Darijani, H., Naghdabadi, R., 2010. Constitutive modeling of solids at finite deformation using a second-order stress-strain relation. International Journal of Engineering Science 48, 223–236.
Duerig, T.W., Melton, K.N., Stoekel, D., Wayman, C.M., 1990. Engineering Aspects of Shape Memory Alloys. Butterworth-Heinemann, London.
Eterovic, A.L., Bathe, K.J., 1990. A hyperelastic-based large strain elasto-plastic constitutive formulation with combined isotropic-kinematic hardening using the logarithmic stress and strain measures. International Journal for Numerical Methods in Engineering 30, 1099–1114.
Evangelista, V., Marfia, S., Sacco, E., 2009. A 3D SMA constitutive model in the framework of finite strain. International Journal for Numerical Methods in Engineering.
Funakubo, H., 1987. Shape Memory Alloys. Gordon and Breach Science Publishers, New York.
Ghavam, K., Naghdabadi, R., 2007. Spin tensors associated with corotational rates and corotational integrals in continua. International Journal of Solids and Structures 44, 5222–5235.
Grabe, C., Bruhns, O., 2009. Path dependence and multiaxial behavior of a polycrystalline niti alloy within the pseudoelastic and pseudoplastic temperature regimes. International Journal of Plasticity 25, 513–545.
Gurtin, M.E., Anand, L., 2005. The decomposition $f = fefp$, material symmetry, and plastic irrotationality for solids that are isotropic-viscoplastic or amorphous. International Journal of Plasticity 21, 1686–1719.
Haupt, P., 2002. Continuum Mechanics and Theory of Materials. Springer Publication House.
Helm, D., 2001. Formgedächtnislegierungen–experimentelle untersuchung, phänomenologische Modellierung und numerische Simulation der thermomechanischen Materialeigenschaften. Ph.D. Thesis. Universitat Gesamthochschule Kassel.
Helm, D., 2007. Thermodynamics of martensitic phase transformations in shape memory alloys. I. Constitutive theories for small and large deformations. Journal of Mechanics of Materials and Structures 2, 87–112.
Helm, D., Haupt, P., 2002. Thermomechanical representation of the multiaxial behavior of shape memory alloys. In: Lynch, C.S. (Ed.), Proceedings of SPIE Smart Structures and Materials 2002. Active Materials: Behavior and Mechanics, vol. 4699, pp. 343–354.
Helm, D., Haupt, P., 2003. Shape memory behaviour: modelling within continuum thermomechanics. International Journal of Solids and Structures 40, 827–849.
Henann, D.L., Anand, L., 2009. A large deformation theory for rate-dependent elastic–plastic materials with combined isotropic and kinematic hardening. International Journal of Plasticity 25, 1833–1878.
Hencky, H., 1928. Über die form des elastizitätsgesetzes bei ideal elastischen stoffen. Zeitschrift fur Technische Physik 9, 214–247.
Holzapfel, G.A., 2000. Nonlinear Solid Mechanics: A Continuum Approach for Engineering. Wiley.
Lagoudas, D.C., Entchev, P.B., 2004. Modeling of transformation-induced plasticity and its effect on the behavior of porous shape memory alloys. Part I: constitutive model for fully dense smas. Mechanics of Materials 36, 865–892.
Leclercq, S., Lexcellent, C., 1996. A general macroscopic description of the thermomechanical behavior of shape memory alloys. Journal of the Mechanics and Physics of Solids 44, 953–957.
Lim, T.J., McDowell, D.L., 1999. Mechanical behavior of an Ni–Ti shape memory alloy under axial-torsional proportional and nonproportional loading. Journal of Engineering Materials and Technology 121, 9–18.
Lin, R.C., Schomburg, U., 2003. A novel internal dissipation inequality by isotropy and its implication for inelastic constitutive characterization. Mechanics Research Communications 30, 125–133.
Lubarda, V.A., 2002. Elastoplasticity Theory. CRC Press.
Miehe, C., 1996. Exponential map algorithm for stress updates in anisotropic multiplicative elastoplasticity for single crystals. International Journal for Numerical Methods in Engineering 39, 3367–3390.
Miehe, C., Apel, N., Lambrecht, M., 2002. Anisotropic additive plasticity in the logarithmic strain space: modular kinematic formulation and implementation based on incremental minimization principles for standard materials. Computer Methods in Applied Mechanics and Engineering 191, 5383–5425.
Moumni, Z., Zaki, W., Nguyen, Q.S., 2008. Theoretical and numerical modeling of solid-solid phase change: application to the description of the thermomechanical behavior of shape memory alloys. International Journal of Plasticity 24, 614–645.
Müller, C., Bruhns, O., 2004. An eulerian model for pseudoelastic shape memory alloys. Materialwissenschaft Und Werkstofftechnik 35, 260–271.
Müller, C., Bruhns, O., 2006. A thermodynamic finite-strain model for pseudoelastic shape memory alloys. International Journal of Plasticity 22, 1658–1682.
Naghdabadi, R., Yeganeh, M., Saidi, A., 2005. Application of corotational rates of the logarithmic strain in constitutive modeling of hardening materials at finite deformations. International Journal of Plasticity 21, 1546–1567.
Ogden, R.W., 1984. Non-Linear Elastic Deformations. Ellis Horwood Limited.
Otsuka, K., Wayman, C.M., 1998. Shape Memory Materials. Cambridge University Press, Cambridge.
Ottosen, N.S., Ristinmaa, M., 2005. The Mechanics of Constitutive Modeling. Elsevier.
Pai, P.F., Palazotto, A.N., Greer Jr., J.M., Greer, J.M., 1998. Polar decomposition and appropriate strains and stresses for nonlinear structural analyses. Computers and Structures 66, 823–840.
Pan, H., Thamburaja, P., Chau, F., 2007a. An isotropic-plasticity-based constitutive model for martensitic reorientation and shape-memory effect in shape-memory alloys. International Journal of Solids and Structures 44, 7688–7712.
Pan, H., Thamburaja, P., Chau, F., 2007b. Multi-axial behavior of shape-memory alloys undergoing martensitic reorientation and detwinning. International Journal of Plasticity 23, 711–732.
Panico, M., Brinson, L., 2007. A three-dimensional phenomenological model for martensite reorientation in shape memory alloys. Journal of the Mechanics and Physics of Solids 55, 2491–2511.
Patoor, E., Eberhardt, A., Berveiller, M., 1996. Micromechanical modelling of superelasticity in shape memory alloys. Journal De Physique IV 6, 277–292.
Peric, D., Owen, D.R.J., Honnor, M.E., 1992. A model for finite strain elasto-plasticity based on logarithmic strains: computational issues. Computer Methods in Applied Mechanics and Engineering 94, 35–61.
Pethö, A., 2001. Constitutive modelling of shape memory alloys at finite strain. Zeitschrift Fur Angewandte Mathematik Und Mechanik 81, 355–356.
Popov, P., Lagoudas, D.C., 2007. A 3D constitutive model for shape memory alloys incorporating pseudoelasticity and detwinning of self-accommodated martensite. International Journal of Plasticity 23, 1679–1720.
Qidwai, M.A., Lagoudas, D.C., 2000. On thermomechanics and transformation surfaces of polycrystalline niti shape memory alloy material. International Journal of Plasticity 16, 1309–1343.
Raniecki, B., Lexcellent, C., 1994. Rl-models of pseudoelasticity and their specification for some shape memory solids. European Journal of Mechanics A – Solids 13, 21–50.
Raniecki, B., Lexcellent, C., 1998. Thermodynamics of isotropic pseudoelasticity in shape memory alloys. European Journal of Mechanics A – Solids 17, 185–205.
Raniecki, B., Lexcellent, C., Tanaka, K., 1992. Thermodynamic models of pseudoelastic behaviour of shape memory alloys. Archive of Mechanics 44, 261–284.
Reese, S., Christ, D., 2008. Finite deformation pseudo-elasticity of shape memory alloys – constitutive modelling and finite element implementation. International Journal of Plasticity 24, 455–482.
Reinhardt, W., Dubey, R., 1996. Application of objective rates in mechanical modeling of solids. ASME Journal of Applied Mechanics 63, 692–698.
Reinhardt, W.D., Dubey, R.N., 1995. Eulerian strain-rate as a rate of logarithmic strain. Mechanics Research Communications 22, 165–170.
Shaw, J.A., 2000. Simulations of localized thermo-mechanical behavior in a niti shape memory alloy. International Journal of Plasticity 16, 541–562.
Sittner, P., Hara, Y., Tokuda, M., 1995. Experimental study on the thermoelastic martensitic transformation in shape memory alloy polycrystal induced by combined external forces. Metallurgical and Materials Transactions A 26, 2923–2935.

Souza, A.C., Mamiya, E.N., Zouain, N., 1998. Three-dimensional model for solids undergoing stress-induced phase transformations. European Journal of Mechanics A – Solids 17, 789–806.
Stein, E., Sagar, G., 2008. Theory and finite element computation of cyclic martensitic phase transformation at finite strain. International Journal for Numerical Methods in Engineering 74, 1–31.
Thamburaja, P., 2005. Constitutive equations for martensitic reorientation and detwinning in shape-memory alloys. Journal of the Mechanics and Physics of Solids 53, 825–856.
Thamburaja, P., 2010. A finite-deformation-based phenomenological theory for shape-memory alloys. International Journal of Plasticity 26, 1195–1219.
Thamburaja, P., Anand, L., 2001. Polycrystalline shape-memory materials: effect of crystallographic texture. Journal of the Mechanics and Physics of Solids 49, 709–737.
Thiebaud, F., Lexcellent, C., Collet, M., Foltete, E., 2007. Implementation of a model taking into account the asymmetry between tension and compression, the temperature effects in a finite element code for shape memory alloys structures calculations. Computational Materials Science 41, 208–221.
Truesdell, C., Noll, W., 1965. The Non-Linear Field Theories of Mechanics. Springer-Verlag.
Vladimirov, I.N., Pietryga, M.P., Reese, S., 2008. On the modelling of non-linear kinematic hardening at finite strains with application to springback-comparison of time integration algorithms. International Journal for Numerical Methods in Engineering 75, 1–28.
Vladimirov, I.N., Pietryga, M.P., Reese, S., 2010. Anisotropic finite elastoplasticity with nonlinear kinematic and isotropic hardening and application to sheet metal forming. International Journal of Plasticity 26, 659–687.
Xiao, H., Bruhns, O.T., Meyers, A., 1997. Logarithmic strain, logarithmic spin and logarithmic rate. Acta Mechanica 124, 89–105.
Xiao, H., Bruhns, O.T., Meyers, A., 2000. A consistent finite elastoplasticity theory combining additive and multiplicative decomposition of the stretching and the deformation gradient. International Journal of Plasticity 16, 143–177.
Xiao, H., Bruhns, O.T., Meyers, A., 2001. Large strain responses of elastic-perfect plasticity and kinematic hardening plasticity with the logarithmic rate: swift effect in torsion. International Journal of Plasticity 17, 211–235.
Xiao, H., Bruhns, O.T., Meyers, A., 2004. Explicit dual stress-strain and strain-stress relations of incompressible isotropic hyperelastic solids via deviatoric hencky strain and cauchy stress. Acta Mechanica 168, 21–33.
Xiao, H., Bruhns, O.T., Meyers, A., 2006. Elastoplasticity beyond small deformations. Acta Mechanica 182, 31–111.
Xiao, H., Chen, L.S., 2002. Hencky's elasticity model and linear stress-strain relations in isotropic finite hyperelasticity. Acta Mechanica 157, 51–60.
Yeganeh, M., Naghdabadi, R., 2006. Axial effects investigation in fixed-end circular bars under torsion with a finite deformation model based on logarithmic strain. International Journal of Mechanical Sciences 48, 75–84.
Ziolkowski, A., 2007. Three-dimensional phenomenological thermodynamic model of pseudoelasticity of shape memory alloys at finite strains. Continuum Mechanics and Thermodynamics 19, 379–398.